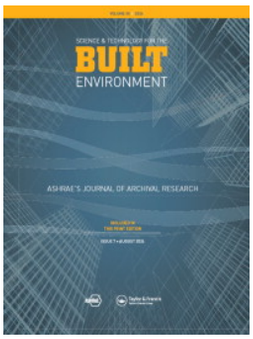

Taylor & Francis
Taylor & Francis Group

Science and Technology for the Built Environment

ISSN: (Print) (Online) Journal homepage: www.tandfonline.com/journals/uhvc21

Improved engineering model for water absorption in softwoods

Samuel V. Glass, Charles R. Boardman, Natalia Farkas, Eleanor Q. D. Lazarcik & Samuel L. Zelinka

To cite this article: Samuel V. Glass, Charles R. Boardman, Natalia Farkas, Eleanor Q. D. Lazarcik & Samuel L. Zelinka (2024) Improved engineering model for water absorption in softwoods, Science and Technology for the Built Environment, 30:7, 694-708, DOI: 10.1080/23744731.2023.2299167

To link to this article: https://doi.org/10.1080/23744731.2023.2299167

Science and Technology for the Built Environment, (2024) **30**, 694–708

ISSN: 2374-4731 print / 2374-474X online
DOI: 10.1080/23744731.2023.2299167

Improved engineering model for water absorption in softwoods

SAMUEL V. GLASS, CHARLES R. BOARDMAN, NATALIA FARKAS, ELEANOR Q. D. LAZARCIK AND SAMUEL L. ZELINKA

Building and Fire Sciences, USDA Forest Service, Forest Products Laboratory, Madison, WI, USA

Modeling of moisture transfer in porous materials is typically partitioned into liquid transport and vapor diffusion. Coefficients for liquid transport are often derived from laboratory measurements of water absorption by partial immersion. Although the assumption that capillary liquid transport is dominant while vapor diffusion is negligible is a reasonable assumption for mineral-based materials, recent work indicates that it is not representative of water absorption in wood across the grain. This article builds on earlier work and develops an improved engineering model for liquid water transport in softwoods. The approach uses a constant liquid diffusivity value, relies primarily on ordinary hygrothermal property measurements, and partitions vapor and liquid transport in a practical way that is informed by current understanding of wood–water interactions. The model is optimized using one-dimensional simulations calibrated against measured water uptake across a range of softwood species. Laboratory measurements were conducted to investigate key properties of eastern white cedar, which had the highest relative error in a previous version of the model, and to examine the practicality and relevance of vacuum saturation and free saturation for southern yellow pine. The model accuracy is improved by paying closer attention to the moisture storage function and capillary saturation value.

Introduction

The building envelope performs multiple roles that are critical for comfortable, healthy, energy efficient and durable buildings. Key performance requirements include prevention of bulk water intrusion and management of heat, air, and moisture (ASHRAE 2019a, 2021b). Moisture levels in buildings affect indoor air quality, the health and comfort of the occupants, and the serviceability of the structure. Indoor dampness and microbial growth have been linked to adverse health effects (IOM 2004; WHO 2009; Mendell et al. 2011), and moisture accumulation can lead to deterioration of structural materials and finishes (ASHRAE 2019a, 2019b, 2021c).

Porous building materials absorb water by capillary action. Exposure to water may occur from precipitation during the construction process prior to enclosure of the building or in the form of wind-driven rain against cladding materials such as brick, stone, stucco, or wood throughout the service life of the building. Liquid water absorption in such materials is commonly measured using standard laboratory methods (ASTM 2019; ISO 2002). The sides of the specimen are sealed with a water-impermeable coating to limit absorption to one surface and the specimen is immersed in water to a depth of a few millimeters, periodically removed, weighed, and immersed again. For many mineral-based materials, a plot of water uptake (kg m^{-2}) versus square root of time is bilinear, as depicted in Figure 1a for ceramic brick. The slope of the initial linear portion (red line in Figure 1a) is known as the water absorption coefficient A (kg m^{-2} $s^{-0.5}$), and the plateau indicates that the material has reached the capillary saturation water content w_c (kg m^{-3}), also known as the free water saturation value.

Wood interacts with water differently from mineral-based materials. Wood undergoes considerable expansion and contraction with changes in moisture content. The transfer of heat, air, and moisture in wood depends on the direction relative to the growth rings (radial vs. tangential) and the longitudinal axis of the tree. For example, liquid water transport and water vapor diffusion are much faster in the longitudinal direction (with the grain) than in the radial or tangential directions (across the grain) (Thybring et al. 2022). Liquid water absorption in wood is typically much slower than in mineral-based materials. This is shown for spruce (across the grain) in Figure 1b; note that the vertical axis for spruce has a 50x zoom compared to brick. The slow rate of water uptake in wood means that the capillary saturation value cannot be determined from a plateau in a partial

Received June 15, 2023; accepted November 27, 2023
Samuel V. Glass, PhD, Full Member ASHRAE, is a Research Physical Scientist. **Charles R. Boardman, MS, Associate Member ASHRAE**, is a General Engineer. **Natalia Farkas, PhD**, is a Research Physical Scientist. **Eleanor Q. D. Lazarcik, MS**, is a Physical Science Technician. **Samuel L. Zelinka, PhD**, is a Project Leader and Materials Research Engineer.
Supplemental data for this article can be accessed online at https://doi.org/10.1080/23744731.2023.2299167.
Corresponding author e-mail: samuel.v.glass@usda.gov

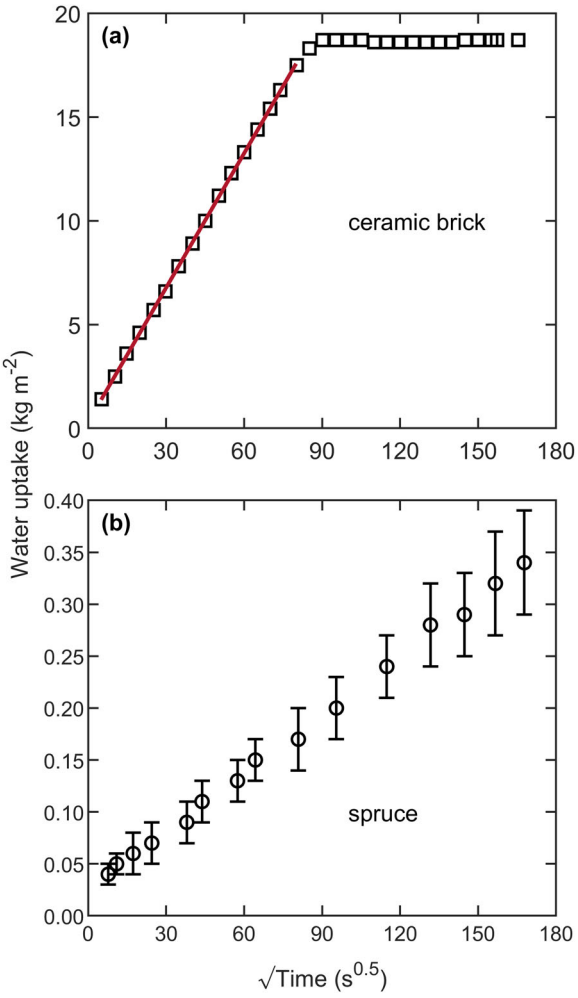

Fig. 1. Measured liquid water absorption in a) ceramic brick (Scheffler et al. (2007) and (b) spruce across the grain (Kumaran et al. 2002). Note the different vertical axis scales.

immersion test within a practical timeframe. While mineral-based materials typically reach a plateau in hours to days, wood can take months or years. Various alternative methods for determining capillary saturation will be discussed later in this article.

Hygrothermal simulation is an important tool for building envelope design analysis; it predicts moisture and temperature conditions over time within multilayer assemblies in response to interior and exterior environmental conditions (Hens 1996; Trechsel 2001; Straube and Burnett 2005; ASTM 2016; ASHRAE 2021a). This type of analysis can help identify and mitigate potential moisture performance risks prior to construction. At the material level, several properties can be specified, such as thickness, bulk density, porosity, specific heat capacity, thermal conductivity, moisture content as a function of relative humidity, and moisture transfer coefficients.

Moisture transfer in porous building materials is typically partitioned by hygrothermal models into two mechanisms: vapor diffusion and liquid transport. A common tacit assumption is that liquid transport is dominant during a water absorption experiment and vapor diffusion is negligible. Models for liquid diffusivity in porous materials range from simplified approximations that rely only on A and w_c (e.g., Künzel 1995; Kumaran 1999) to more detailed models with many more parameters (e.g., Carmeliet, Janssen, and Derluyn 2007; Scheffler et al. 2007). The approximation proposed by Künzel (1995), which is used in the hygrothermal model WUFI (Wärme Und Feuchte Instationär or "transient heat and moisture transfer"; IBP 2022), expresses the liquid transport coefficient for suction D_w (m^2 s^{-1}) as a function of water content w (kg m^{-3}) as follows:

$$D_w(w) = 3.8 \left(\frac{A}{w_c}\right)^2 1000^{w/w_c - 1} \quad (1)$$

Calculations using this approximation give reasonable agreement with measurements for natural stone materials, both for water uptake vs. square root of time and water content profiles at different times during the absorption process (Krus 1996). Further details on how this approximation is used in the overall model for heat and moisture transfer can be found elsewhere (Künzel 1995; Künzel and Kiessl 1997).

Equation (1) has been applied to many materials in the WUFI North America Database (IBP 2022), including five wood species. The material properties are based on laboratory measurements from ASHRAE Research Project 1018 (Kumaran et al. 2002). At a basic level, when hygrothermal property data are implemented in a model and the laboratory measurements are simulated using the same boundary conditions, the output of a valid model should match the measurements. However, recent work has demonstrated that Equation (1) is inaccurate for modeling water absorption in wood (Kordziel et al. 2020; Glass, Boardman, and Daniels 2022). For illustration, the simulated water absorption experiment using properties for spruce from the WUFI North America Database is compared with the laboratory measurements reported by Kumaran et al. (2002) in Figure 2 (see Supplementary Material Part I for details on all five wood species). The simulation using original database properties vastly overpredicts the rate of water uptake compared with measured data. In this case, simulated liquid transport is based on Equation (1) with the assumption that the measured A value reflects liquid only, while simulated vapor diffusion is based on independent steady-state vapor transmission measurements. The simulation in which vapor diffusion is effectively excluded matches the measurements, indicating that Equation (1) would be accurate if vapor diffusion were negligible. However, a simulation in which liquid transport is excluded clearly indicates that vapor diffusion is not negligible, explaining the overprediction of the original simulation. This example highlights the need to create independent models for wood and mineral-based materials. All in all, wood is not just another brick in the wall.

Although wood behaves differently from mineral-based materials, the systematic overprediction of water uptake in wood discussed above does not stem from oversimplifying physical phenomena. We acknowledge that wood exhibits complex features, such as non-linear liquid water uptake vs. square root of time (Zillig 2009; Sedighi-Gilani et al. 2012, 2014; Zelinka et al. 2016b). In addition, the kinetics of water

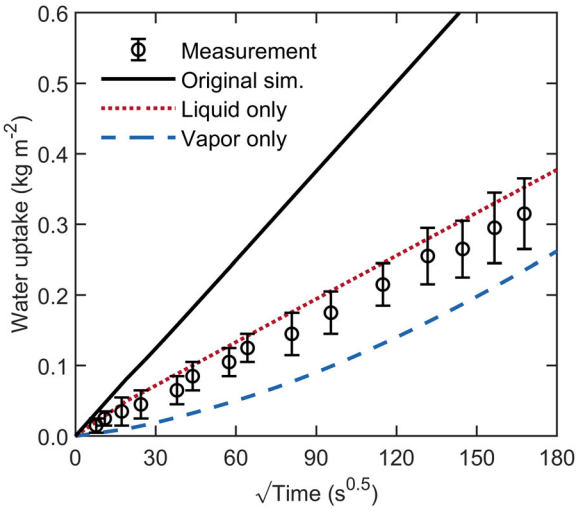

Fig. 2. Water absorption measurements for spruce (Kumaran et al. 2002) compared with simulation for the same material from the WUFI North America Database ("Original sim."), simulation with vapor diffusion excluded ("Liquid only") by making the vapor diffusion resistance factor arbitrarily large, and simulation with liquid transport excluded ("Vapor only").

vapor sorption in wood are non-Fickian at small length scales (e.g., Christensen and Kelsey 1959; Wadsö 1994; Thybring, Glass, and Zelinka 2019, Thybring et al. 2022). Despite these complexities, moisture transfer in wood can still be approximated reasonably well for practical applications at the building envelope scale.

We recently developed an improved model for water absorption in wood (Glass, Boardman, and Daniels 2022). This approach does not require data beyond ordinary hygrothermal property measurements, avoids the incorrect assumption that vapor diffusion is negligible during liquid water uptake measurements, and partitions vapor and liquid transport in a practical way guided by current understanding of wood–water interactions. The model was calibrated by comparing simulations with measured water uptake using literature data for a range of softwood species. Six out of nine species had relative errors of 3% or less. The species with the largest relative error (63%) was eastern white cedar, and further work was recommended to investigate this possible outlier. Further measurements were also recommended for capillary saturation, given the lack of data in the literature.

In this article we improve this model, investigate the hygrothermal properties of eastern white cedar with laboratory measurements, conduct free saturation and vacuum saturation measurements over time for southern yellow pine to examine their practicality and relevance for modeling, and conduct a more detailed analysis of the moisture storage function for each wood species, paying particular attention to the effective capillary saturation value for water absorption across the grain. The following section provides relevant background on the current understanding of wood–water interactions used to develop the model. Next, we describe our laboratory measurements, the data mined from the literature, the structure of the engineering model, and its optimization. Finally, we present measurement results, show that the model improves simulation accuracy, and identify topics that need further research.

Background

Types of water in wood

Wood cell walls are composed of biopolymers including ordered cellulose, amorphous cellulose, hemicelluloses, and lignin. Water can be present within the cell wall and in the capillary volume, which includes the lumen and features such as the chambers of bordered pits, as depicted in Figure 3. Water molecules in the cell wall interact with the hydroxyl (OH) groups of the wood polymers through hydrogen bonding (Chen et al. 2018, Plaza 2019). Water molecules increase the volume of the cell wall, which is reflected in macroscopic swelling and shrinkage of wood with changes in moisture content. We refer to this type of water as *cell wall water* (the term *bound water* is also commonly used). Cell wall water does not undergo a freezing/melting phase transition at temperatures as low as −65 C based on differential scanning calorimetry (DSC) measurements (Zelinka et al. 2012). In contrast to cell wall water, the DSC data indicate that *capillary water* within the porous microstructure of wood undergoes a freezing/melting transition like liquid water. Although the term *free water* has often been used in the literature, its use is not encouraged because capillary water interacts with the internal surfaces of wood cells and is thermodynamically different from pure liquid water (Fredriksson 2019; Thybring et al. 2022).

Moisture storage function

The moisture storage function describes the relationship between moisture content and relative humidity (RH) at equilibrium over the full moisture range. Here, moisture content u (kg kg^{-1}) refers to the mass ratio of water to dry solid material; it is also commonly expressed as a percentage and abbreviated MC. Water content w (kg m^{-3}) refers to the ratio of the mass of water to the bulk volume of the solid material and is the product of u and bulk dry density. The moisture content of wood increases dramatically at high RH. Given that this article focuses on modeling water absorption, the subsequent discussion does not address sorption hysteresis or desorption.

Measurements in softwoods indicate that water is predominantly located in the cell walls up to RH levels above 99%; in most cases, the amount of capillary water is negligible below 99% RH (Thygesen, Engelund, and Hoffmeyer 2010; Fredriksson 2019). For example, DSC measurements did not detect any capillary water in Douglas-fir equilibrated (by absorption from a dry initial condition) at 95% RH, and at 99.65% RH the amount of capillary water was less than 0.004 kg kg^{-1} (Fredriksson and Thybring 2019). Calculations based on softwood anatomical features including bordered pits and the pointed ends of tracheids predict a contribution from capillary water of about 0.0001 kg kg^{-1} at 99% RH, increasing to just under 0.0035 kg kg^{-1} at 99.9% RH

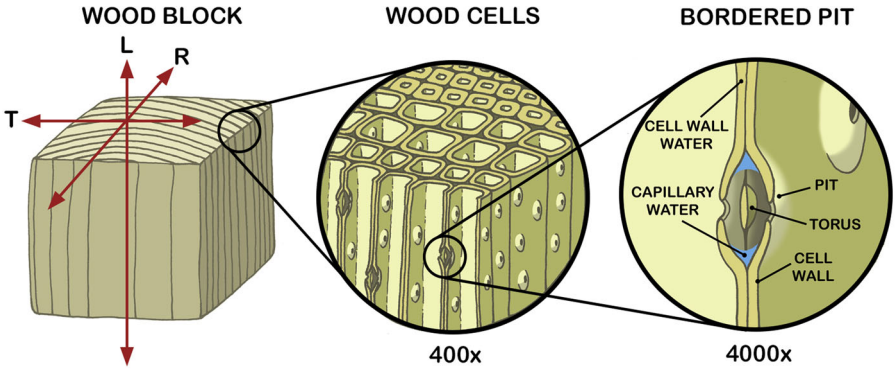

Fig. 3. Generic softwood block (left) showing longitudinal (L), radial (R), and tangential (T) axes; magnified cellular structure (middle) for a section through the center of the block; and magnified structure of a bordered pit (right). Cell wall water is located inside the solid cell walls and forms hydrogen bonds with hydroxyl groups of the wood polymers. Capillary water is located in the porous microstructure.

(Engelund, Thygesen, and Hoffmeyer 2010). This value at 99.9% RH is roughly consistent with the measurements quoted above. As RH increases above 99.9%, the amount of capillary water increases rapidly, corresponding to filling of the pore structure.

Maximum saturation

Although maximum saturation is usually not relevant for water absorption in building applications, it can be used for determining the porosity of the material, which is typically specified as a material property in hygrothermal models. Maximum saturation is reached when the whole capillary volume is filled with water and is typically measured with samples submerged in water under vacuum. Theoretical maximum saturation u_{max} (kg kg^{-1}) of wood can be calculated using the dry bulk density ρ_0 (kg m^{-3}) as shown in the Supplementary Material Part II:

$$u_{\max} = \frac{1000}{\rho_0} - 0.3844 \tag{2}$$

This can also be expressed as maximum water content w_{max} (kg m^{-3}):

$$w_{\max} = 1000 - 0.3844\rho_0 \tag{3}$$

The porosity φ ($= w_{\max}/1000$) can then be calculated as

$$\varphi = 1 - \frac{0.3844\rho_0}{1000} \tag{4}$$

Capillary saturation

Mineral-based materials often reach capillary saturation within a practical amount of time after starting a partial immersion test (see Figure 1a). This is not the case, however, for water uptake in wood across the grain. Capillary saturation is generally less than maximum saturation because of entrapped air within the pore structure. Another method for determining capillary saturation is with advanced imaging techniques that measure the moisture content as a function of distance from the wetted surface over time. Several studies have measured moisture profiles in wood during water absorption with techniques such as gamma ray attenuation, nuclear magnetic resonance (NMR), neutron radiography, and X-ray computed tomography (Krus and Vik 1999; Kumaran 1999; Sandberg and Salin 2012; Sedighi-Gilani et al. 2012, 2014; Gezici-Koç et al. 2017). Capillary saturation can be defined as the moisture content just above the wood–water interface. For water uptake along the grain, imaging methods cited above yield capillary saturation values for softwoods in the range 1.5–2 kg kg^{-1} or 650–900 kg m^{-3}. This range is nearly the same as maximum saturation, which can be explained based on wood structure. Axial tracheids, the most common type of cell in softwoods, generally have a length in the range 1–10 mm (Wiedenhoeft 2021). At an end-grain surface, water readily fills the voids of the cut cells. The imaging techniques mentioned above typically have spatial resolution finer than 1 mm, so they detect the filling of the cut cells.

The situation is different for water absorption across the grain. Axial tracheids generally have a diameter less than 1% of their length (Wiedenhoeft 2021), so the complete filling of cut cells near the wood–water interface has a limited effect spatially. Two of the studies mentioned above reported moisture profiles for water uptake across the grain. Sedighi-Gilani et al. (2014) found an effective saturation value of around 400 kg m^{-3} for water uptake in Scots pine sapwood in the tangential direction. The mean dry bulk density was 450 kg m^{-3}, so the effective saturation value was about 0.9 kg kg^{-1}. This value is about half of maximum saturation. Gezici-Koç et al. (2017) imaged water absorption in Scots pine sapwood in the radial direction over a longer duration using NMR. They found that the moisture content near the wood–water interface increased over time but was limited to about 0.8 kg kg^{-1} in the first 21 days. In addition to giving the total moisture content, NMR can separate cell wall water from capillary water. A notable finding of this study is that the cell wall water content rises spatially through the specimen ahead of capillary water (Gezici-Koç et al. 2017). The likely mechanism is diffusion of water vapor through the pore structure combined with sorption in the cell walls and diffusion of the cell wall water.

Water vapor transmission

Water vapor transmission through wood increases with increasing relative humidity. The vapor permeability and vapor diffusion resistance factor for select wood species are plotted in Figure 4. The water vapor diffusion resistance factor (or μ-value) is the ratio of the vapor permeability of still air (diffusion with no convection) to that of the material. The observed trends reflect the increase in mobility of cell wall water with increasing RH (Thybring et al. 2022). The primary pathway is diffusion of water vapor through the pore structure, but this usually does not provide a continuous path. Water molecules must cross the cell wall (or pass through bordered pits or other features) to get to the next void. As RH increases, the cell wall water content increases, which swells the cell wall, increases its porosity and the connectivity of water molecules (Kulasinski et al. 2015), and softens the amorphous polymers (Jakes et al. 2019). Additionally, the strength of attraction between water and cell wall polymers decreases as RH increases (Nopens et al. 2019), thereby increasing water mobility.

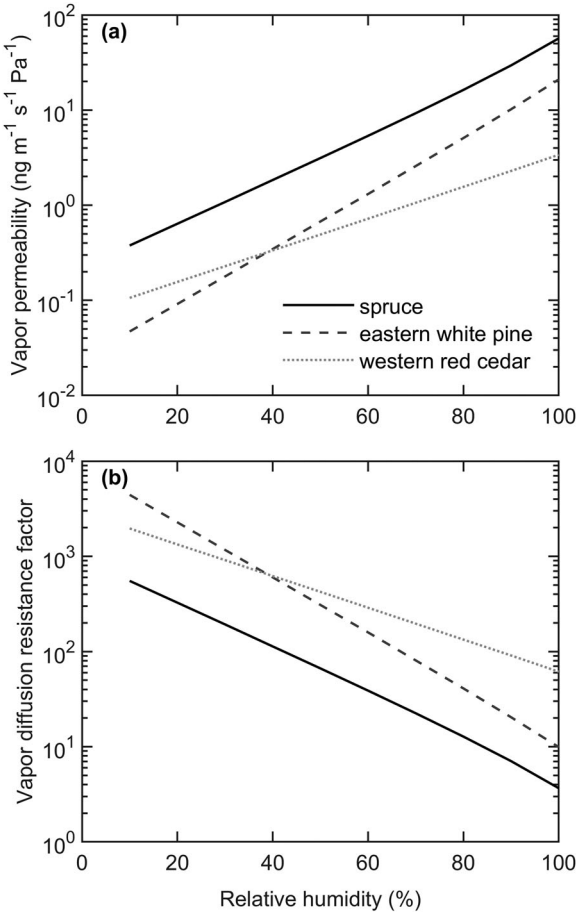

Fig. 4. Semi-log plots of (a) derived vapor permeability and (b) calculated vapor diffusion resistance factor vs. RH for three wood species (Kumaran et al. 2002).

Materials and methods

Laboratory measurements

Measurements were taken for eastern white cedar (EWC) and southern yellow pine (SYP). Eastern white cedar, also known as northern white-cedar (*Thuja occidentalis*), was selected because previous work (Glass, Boardman, and Daniels 2022) indicated that this species was an outlier when the liquid diffusivity from a predictor equation was compared with that from a calibrated simulation. EWC boards were obtained from a local building material supply and were originally either 20 mm or 25 mm thick across the grain. Photographs of EWC specimens cut and sanded to 16 mm thickness for different types of measurements are shown in Figure 5. Additionally, select measurements were made using the same SYP specimens studied by Zelinka et al. (2016b) to acquire data on vacuum saturation and free saturation over longer duration. The term "species" in this article in some contexts is consistent with botanical taxonomy (e.g., *Thuja occidentalis*) but is also used for commercial groups that include multiple species, such as the SYP group.

Dry bulk density was determined using Method A of ASTM D2395 (ASTM 2017) for EWC specimens either 50 50 16 mm or 100 50 16 mm. Mass was measured with an electronic balance (±0.001 g) after drying in an environmental chamber at 76 ± 1 C near 0% RH for a minimum of 24 h (subsequent measurements at 48 h changed by no more than 0.1%). Dimensions were measured with a digital caliper (±0.01 mm).

Vacuum saturation was measured for 50 50 mm EWC specimens that were 2.5, 5, or 16 mm thick across the grain, with six replicates of each thickness. All surfaces were

Fig. 5. Photographs of select eastern white cedar specimens for liquid water absorption measurements (a), sorption isotherm measurements (b), and water vapor transmission measurements (c).

sanded smooth. Specimens were placed in deionized water and held under vacuum (3.0 kPa absolute pressure) for 10 days. After 3, 5, and 10 days, specimens were taken out of the water, blotted with a moist cloth to remove droplets, and weighed. They were placed in water again without vacuum for another 10 days. Dimensions in the saturated state and dry mass and bulk density were measured according to the procedure given above.

Free saturation and vacuum saturation were measured for 50 50 mm SYP specimens that were 6, 12, or 18 mm thick in each of the three anatomical directions (longitudinal, radial, and tangential), with three replicates each. Free saturation was measured by placing samples in deionized water without applying vacuum or pressure. Initially the samples floated but became fully submerged once they absorbed sufficient water. Samples were periodically removed, blotted, and weighed until the rate of change in mass based on five or more points spaced over a one-month period was less than 10 mg day^{-1}, which is small relative to the repeatability error (±0.1 g from blotting). Some specimens took up to a year to reach this criterion. Vacuum saturation measurements followed the same procedure above for EWC, but the duration for SYP specimens was limited to 5 days.

The moisture storage function in the hygroscopic range (sorption isotherm) was characterized using two methods. The first accommodated six EWC replicates simultaneously using a custom chamber in which RH was regulated by a constant-flow humidity generator (Zelinka et al. 2018a). Specimens 50 50 mm with a thickness of 16 mm across the grain were pre-dried at 76 ± 1 C near 0% RH for 24 h. Targeted conditions were 50%, 80%, and 90% RH at 23 C. RH sensor measurement uncertainty was ±1% RH, and temperature stability was ±1.1 C. Equilibrium was operationally determined by continuously monitoring the mass of one specimen *in situ* with an electronic balance (±0.1 mg) until the rate of change in mass was less than 12 mg over 24 h (<0.1% of dry mass per day). After this criterion was reached, the mass of each specimen was measured using the same balance. After equilibration at the final RH setting, specimens were dried again at 76 ± 1 C for 48 h. Initial and final dry masses differed by no more than 0.1%.

The second method used an automated gravimetric sorption analyzer (IGAsorp, Hiden Isochema, Warrington, UK), which has a microbalance with 0.1 μg resolution. Inherent mass instability from random noise, vibration, and drift was previously found to be less than 2 μg over 24 h (Glass et al. 2018). EWC specimens were cut with approximate dimensions of 1.2 mm in the longitudinal direction and 8 mm in the radial and tangential directions, having dry mass between 19 and 22 mg. Three replicates were run sequentially. The sample was placed in a stainless-steel mesh basket suspended from the microbalance and was dried under flow of high purity nitrogen at 60 C for 8 h and then thermally equilibrated under nitrogen flow at 25.00 ± 0.02 C, after which dry mass was recorded. RH set points were 10% to 90% at intervals of 10%, followed by a final point at 95% RH. The RH was controlled by mixing dry and water vapor-saturated nitrogen gas streams at a total flow rate of 250 mL/min using electronic mass flow controllers. RH within the sample chamber was calibrated using reference saturated salt solutions (Greenspan 1977), yielding measurement uncertainty of ±0.5% RH. At each RH level, data collection was stopped when the rate of change in mass with time (relative to the dry mass) was less than 5 μg g^{-1} min^{-1} over a 60 min window. Equilibrium moisture content (EMC) was calculated using the correction method of Glass et al. (2018), which is based on an empirical relationship between EMC measured at extended times and MC measured when the criterion mentioned above was attained (relative change in mass with time). Uncertainty in EMC using this method is approximately ±0.002 kg kg^{-1}.

Water vapor transmission was measured using the cup method (ASTM 2022). EWC specimens approximately 168 115 16 mm were edge-coated with neoprene paint (Product N-700A, Republic Powdered Metals, Inc., Medina, OH) and sealed with butyl tape (C.R. Laurence Co., Inc., Los Angeles, CA) to the face of a Pyrex dish containing either A3 molecular sieve desiccant (0% RH) or deionized water (100% RH). The direction of vapor transmission was across the grain. The dish assemblies were placed in an environmental chamber at 23 C and constant RH measured to an accuracy of ±2% RH. Relative humidity conditions across the specimens (dish/chamber) included 0%/64%, 100%/53%, and 100%/83%. Each dish assembly was removed briefly from the chamber and weighed (±0.01 g) at 24 h intervals until steady state was reached. The vapor permeability δ_p (kg m^{-1} s^{-1} Pa^{-1}) of the specimen was calculated as

$$\delta_p = \frac{\dot{m} \quad l}{S \quad \Delta p_v} \tag{5}$$

where $\dot{m}$ is the steady-state mass transfer rate (kg s^{-1}), l is the specimen thickness (m), S is the exposed surface area of the specimen (m^2), and Δp_v is the difference in vapor pressure across the specimen (Pa). The vapor diffusion resistance factor μ was calculated as

$$\mu = \frac{\delta_a}{\delta_p} \tag{6}$$

where δ_a is the vapor permeability of still air (201 ng m^{-1} s^{-1} Pa^{-1} for the lab conditions of 23 C and barometric pressure of 98.6 kPa). Measurements were corrected to account for still air diffusion resistance (inside the dish) and surface resistances on both sides of the specimen, as stipulated in the standard (ASTM 2022).

Liquid water absorption was measured by partial immersion (ASTM 2019). Twelve replicates of EWC, each 100 50 16 mm, were oriented such that water absorption was across the grain. Specimen edges were sealed using neoprene paint, which had been found in prior work to be impermeable to water and suitable for wood specimens that swell with water uptake (Zelinka, Glass, and Boardman 2016a). After pre-conditioning at 50% RH, specimens were immersed 5 mm in a tray of deionized water. Specimens were removed periodically, blotted with a moist cloth to remove droplets, and weighed (±0.001 g) at the following

intervals: 5 min, 15 min, 30 min, 1, 2, 4, 8, and 24 h, and then daily for a week. The water absorption coefficient was determined from a linear regression of water uptake vs. square root of time for the first 24 h of data.

Literature hygrothermal property data

Measured water absorption data and additional hygrothermal property data for various wood species were obtained from three primary literature sources (Table 1). None of these sources measured capillary saturation directly. Given the lack of data, a value of 0.9 kg kg^{-1} was assigned for all wood species based on imaging studies of water absorption in softwoods across the grain (see Background/Capillary saturation). Furthermore, the moisture storage function for all species was modified to better align with literature measurements. In the hygroscopic range, additional sources were used (Table 1) and empirical curve fitting to data was performed using the ABC isotherm equation (Zelinka, Glass, and Thybring 2018b).

None of the primary literature sources included data measured in absorption in the over-hygroscopic range. Only a few such datasets exist for softwoods (Fortin 1979; Fredriksson and Johansson 2016; Fredriksson and Thybring 2019), the most extensive being that of Fortin (1979) for western hemlock sapwood. Given the lack of data, the moisture storage function for all species in the over-hygroscopic range was based on tension plate data of Fortin (1979). The following points were used: (99.927% RH, 0.319 kg kg^{-1}); (99.963% RH, 0.328 kg kg^{-1}); (99.993% RH, 0.540 kg kg^{-1}).

WUFI software uses linear interpolation between tabulated data points for the moisture storage function (IBP 2022). In the original WUFI database files (Kumaran et al. 2002), there is a gap between the data point at about 89% RH and another value from pressure plate data at 99.78%–99.92% RH, as shown in Figure 6 for SYP and WRC. Linear interpolation in these cases does not correctly represent the moisture storage function. The revised curves include data points based on literature sources at 90%, 95%, and 99% RH such that linear interpolation gives a more accurate representation of the shape.

For all wood species, porosity was calculated from Equation (4). The specific heat capacity was set to 1237 J kg^{-1} K^{-1} based on the *Wood Handbook* (Glass and Zelinka

Table 1. Wood species and data sources.

Wood species	Abbreviation	Primary data source[a]	Sorption isotherm source
Eastern white cedar	EWC1	This work	This work
Eastern white cedar	EWC2	Kumaran et al. (2002)	This work
Western red cedar	WRC	Kumaran et al. (2002)	Hedlin (1967)
Eastern white pine	EWP	Kumaran et al. (2002)	Glass, Zelinka, and Johnson (2014)
Southern yellow pine	SYP1	Kumaran et al. (2002)	Glass, Zelinka, and Johnson (2014)
Spruce	Spruce	Kumaran et al. (2002)	Hedlin (1967)
Southern yellow pine, radial	SYP2 rad.	Zelinka et al. (2016b)	Glass, Zelinka, and Johnson (2014)
Southern yellow pine, tangential	SYP2 tang.	Zelinka et al. (2016b)	Glass, Zelinka, and Johnson (2014)
Douglas-fir	DF	Kordziel et al. (2020)	Hedlin (1967); Kordziel et al. (2020)
Western spruce-pine-fir group	SPF	Kordziel et al. (2020)	Hedlin (1967); Kordziel et al. (2020)

[a]Dry bulk density, water vapor transmission data, and liquid water absorption data.

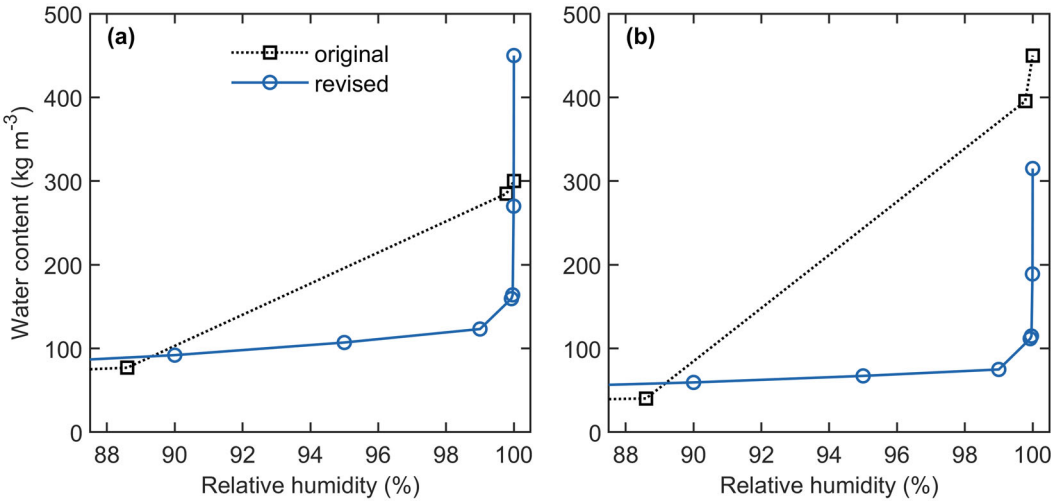

Fig. 6. Original and revised moisture storage functions in the high RH range for (a) southern yellow pine and (b) western red cedar.

2021) at 20 C. The thermal conductivity in the dry state and the moisture-dependent supplement were calculated based on the *Wood Handbook* using dry density, and the default temperature-dependence was used ($0.0002\,\mathrm{W\ m^{-1}\ K^{-2}}$). The RH-dependence of the vapor diffusion resistance factor based on each original literature source was retained. No further changes were made to the hygrothermal properties other than D_w as described below. The complete properties of each wood species are given in detail in the Supplementary Material Part III.

The experimental A-value for each wood species was identified as the slope of a linear regression of water uptake vs. square root of time based on data points during the initial 24 h (or all data points if duration was less than 24 h). The regression was not forced through the origin; this provided the best overall fit to linear and non-linear data.

Model development

The engineering model for liquid transport described here is intended to apply to a range of softwood species. The model framework should be consistent with the fundamental physics covered in the Background, and model predictions should give reasonable agreement with measurements. Our preference is to limit the number of model parameters and to use material property inputs that are readily available. Although Kordziel et al. (2020) found that Equation (1) could be empirically modified to give agreement between simulations and measurements, they did not consider the fundamental physics.

Our approach was informed by an interlaboratory study of water uptake in wood summarized by Kumaran (1999). Matched wood specimens were studied with advanced imaging techniques and analysis methods, but different laboratories arrived at liquid diffusivity functions having highly dissimilar shape and magnitude. Kumaran (1999) suggested that a simple constant diffusivity, independent of water content, would be suitable for practical analysis:

$$D_w \quad \frac{A}{w_c}^{\ 2} \tag{7}$$

This equation served as a starting point. Based on literature data for softwoods, we selected water content at 99% RH as the threshold for liquid transport (see Background/Moisture storage function) and used an RH-dependent water vapor diffusion resistance factor (μ-value) up to 90% RH (see Background/Water vapor transmission). We made the μ-value constant between 90% and 100% RH because water vapor transmission measurements are rarely made above a mean RH of 90% (which corresponds to wet cup at 100% RH and chamber at 80% RH), making extrapolation above this value uncertain.

The relatively slow uptake of water in wood across the grain, together with the observation that vapor diffusion is not negligible in simulations (Figure 2), implies that the experimentally measured A-value reflects both liquid and vapor transport. This is confirmed by NMR measurements indicating that the cell wall water content rises spatially ahead of the capillary water content (Gezici-Koç et al. 2017). In our framework, vapor transport (with RH-dependent μ-value) includes diffusion of water vapor in the capillary volume coupled with diffusion of cell wall water. If the liquid diffusivity is calculated from the experimental A-value and the simulation separately includes vapor transport, the simulation would effectively be double counting the vapor diffusion contribution. Therefore, we use a term like Equation (7) to represent total water transport and subtract an effective vapor diffusion term. Before presenting the equation, we review the origin of Equation (7).

During the initial period in which water uptake varies linearly with square root of time, the normalized change in water content can be expressed as (e.g., Stamm 1964; Siau 1984)

$$\frac{w(t) - w_i}{w_c - w_i} = \sqrt{\frac{4Dt}{\pi l^2}} \tag{8}$$

where $w(t)$ is the average water content ($\mathrm{kg\ m^{-3}}$) as a function of time t (s), w_i is the initial water content ($\mathrm{kg\ m^{-3}}$) assumed to be uniform throughout the material, w_c is the water content of the material at the boundary in contact with liquid water (i.e., capillary saturation, $\mathrm{kg\ m^{-3}}$), D is the diffusion coefficient ($\mathrm{m^2\ s^{-1}}$) representing total water transport, and l is the thickness of the material (m). Let $U(t)$ be the water uptake ($\mathrm{kg\ m^{-2}}$), that is, the mass of water per unit area that has passed through the surface of the material at time t. $U(t)$ is equivalent to $l\,[w(t) - w_i]$ (i.e., the product of thickness and change in average water content). From Equation (8) it follows that

$$U(t) = l[]w(t) - w_i \ = (w_c - w_i)\sqrt{\frac{4Dt}{\pi}} = A\sqrt{t} \tag{9}$$

where A is the water absorption coefficient ($\mathrm{kg\ m^{-2}\ s^{-0.5}}$). Solving this equation for D, we have

$$D = \frac{\pi}{4} \quad \frac{A}{w_c - w_i}^{\ 2} \tag{10}$$

Given our assumption that this total diffusion coefficient is the sum of a liquid diffusivity D_w and vapor diffusivity D_v, we express D_w as

$$D_w = \frac{\pi}{4} \quad \frac{A}{w_c - w_i}^{\ 2} - D_v \tag{11}$$

Here D_v is based on the gradient in water content as the driving potential. It is related to the vapor diffusion resistance factor through

$$D_v \frac{dw}{dx} = \frac{\delta_a}{\mu}\frac{dp_v}{dx} \tag{12}$$

where x is distance (m). From the definition of relative humidity ($h = p_v/p_{vs}$), where p_{vs} is saturation vapor pressure (Pa), at constant temperature it can be shown that

$$D_v = \frac{\delta_a p_{vs}}{\mu\ \frac{\mathrm{d}w}{\mathrm{d}h}} \tag{13}$$

where $(\mathrm{d}w/\mathrm{d}h)$ is the slope of the moisture storage function. Although both μ and $(\mathrm{d}w/\mathrm{d}h)$ vary nonlinearly with h, as a

first approximation, the product of the two quantities is treated as a constant. Given further uncertainty about the interaction between liquid and vapor transport mechanisms, we reduce Equation (13) to an empirical form and write Equation (11) as

$$D_w = \frac{\pi}{4}\left(\frac{A}{w_c - w_i}\right)^2 - \frac{k}{\mu_{90}} \tag{14}$$

where k is a fitting parameter and μ_{90} is the value of the vapor diffusion resistance factor at 90% RH. Eq. (14) resembles the model of Glass, Boardman, and Daniels (2022) but the origin of the first term is clarified and one of the empirical parameters is eliminated.

For practical modeling of the water absorption process in softwoods across the grain, until better data becomes available, we suggest an effective capillary saturation value of 0.9 kg kg^{-1} based on imaging studies (see Background/Capillary saturation); that is, $w_c = 0.9\rho_0$. In the laboratory measurements of water absorption used for model evaluation, the initial water content w_i is the equilibrium value at 50% RH.

Water uptake simulations

Water uptake in each wood species was simulated using WUFI Pro software, version 6.6.0 (IBP 2022). The material thickness was based on reported values in each literature source. A fine numerical grid (100 elements) was generated with the Automatic (II) setting. The initial condition was 50% RH and 22 C. The bottom surface boundary condition was 100% RH and "measured rain" of 5 kg m^{-2} h^{-1}, with a rain exposure factor of 1.0, a rain deposition factor of 1.0, and an adhering fraction of rain of 1.0 to ensure an excess supply of water like the partial immersion test. The bottom surface heat transfer resistance was set to 0 m^2 K W^{-1}. Radiation was not included. The top surface boundary condition was the same temperature and RH as the initial condition, with a surface heat transfer resistance of 0.125 m^2 K W^{-1} and a mass transfer resistance corresponding to a vapor barrier (s_d-value of 100 m) to reflect the laboratory test, where the top surface of the specimen is covered to prevent evaporation. The liquid transport coefficient for suction (D_w) was set to a constant initial value estimated from Equation (7), beginning at the water content corresponding to 99% RH (see Background/Moisture storage function) up to capillary saturation. Simulated water uptake was calculated as the difference between total water content (kg m^{-2}) for each hour and the initial total water content (at time = 0). The value of D_w was calibrated by trial and error such that the slope of the simulated water uptake vs. square root of time matched the experimental A-value.

Model optimization

The fitting parameter k in Equation (14) was optimized as follows, using an initial estimate of 0. The range of D_w values spanned about three orders of magnitude, so our optimization used relative errors rather than absolute errors. The relative error for each wood species, e_j, was calculated as

$$e_j = \frac{D_j^{eqn} - D_j^{cal}}{D_j^{cal}} \tag{15}$$

where D_j^{cal} is the calibrated value of D_w found by simulation and D_j^{eqn} is the value of D_w calculated with Equation (14). The mean relative error, $\overline{e}$, was calculated as

$$\overline{e} = \frac{1}{j}\sum_j |e_j| \tag{16}$$

The Excel Solver (Microsoft Corp., Redmond, WA, USA) was used to identify the value of k in Equation (14) that minimized the mean relative error over all wood species considered in this study.

Results and discussion

Eastern white cedar measurements

The dry bulk density of EWC was 345 ± 12 kg m^{-3} (mean ± standard deviation). The calculated porosity based on this dry density using Equation (4) is 0.867, and the theoretical maximum saturation from Equation (2) is 2.51 kg kg^{-1}. Vacuum saturation measurements for 2.5 mm thick and 5 mm thick specimens are plotted in Figure 7 as a function of time. As expected, the thinner specimens approached saturation faster than the thicker specimens. After 20 days, the mean values of the two groups converged at 2.52 (± 0.13) kg kg^{-1}, slightly greater than the theoretical value. In comparison, a dry bulk density of 360 ± 20 kg m^{-3} was reported by Kumaran et al. (2002), and the vacuum saturation value was 2.28 ± 0.10 kg kg^{-1} for 6 mm thick EWC specimens. The long time needed to saturate the specimens under vacuum is indicative of the low permeability of EWC to liquid water, which is consistent with the relatively low water

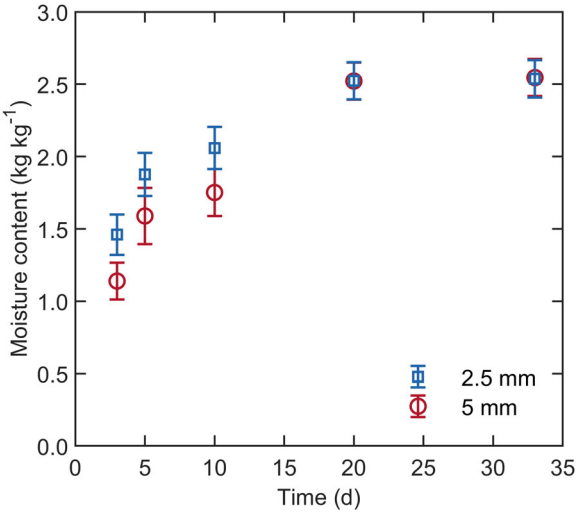

Fig. 7. Moisture content vs. time for vacuum saturation of eastern white cedar specimens of two thicknesses. Error bars represent standard deviation of six replicates.

absorption coefficient (discussed below). However, the vacuum saturation value is not used in any subsequent modeling because it does not accurately represent the capillary saturation value.

Sorption isotherm data are plotted in Figure 8 for small specimens measured with the automated sorption analyzer and large specimens measured with the custom chamber. The coefficient of variation was in the range 0.7%–1.9% for small specimens (three replicates) and 5.1%–8.7% for large specimens (six replicates), reflecting greater inhomogeneity across that sample. The mean equilibrium moisture content across both samples at each RH level (10%–95% RH) was used as input for hygrothermal simulations, with the curve fit providing an estimate at 99% RH. In comparison, the reported moisture content values of Kumaran et al. (2002) are considerably lower (Figure 8).

The water vapor permeability of EWC as a function of RH is compared with reported values from Kumaran et al. (2002) in Figure 9. Our dry cup value (0–64% RH) is the same as Kumaran's dry cup value for 0–71% RH within measurement error. However, Kumaran's dry cup values for 0–50% RH and 0–71% RH differ by an order of magnitude. The reason for this discrepancy is not clear. The estimated uncertainty in Kumaran's derived vapor permeability values (simultaneously fitting all the data) was reported to be 60%. Given the good agreement between our measurements and Kumaran's above 50% RH, we used Kumaran's derived vapor permeability values in the water absorption simulations for both EWC1 and EWC2.

Water absorption in EWC based on the partial immersion test is plotted vs. square root of time in Figure 10. The linear regression yields $A = 1.25\,\mathrm{g\ m^{-2}\ s^{-0.5}}$, which is slightly lower than the value of $1.45\,\mathrm{g\ m^{-2}\ s^{-0.5}}$ based on the data of Kumaran et al. (2002).

In summary, the bulk density, water vapor permeability, and water absorption coefficient of EWC measured in this work are similar to those reported by Kumaran et al. (2002). However, the moisture storage functions differ considerably.

Southern yellow pine measurements

The density of individual SYP specimens showed considerable variation. A relationship between free saturation measurements (long duration) and dry bulk density was observed, as depicted in Figure 11. All measurements are essentially at or below the theoretical maximum saturation (dotted curve). Individual data points were between 92% and 100% of theoretical maximum saturation, with a mean of 96%. Some specimens

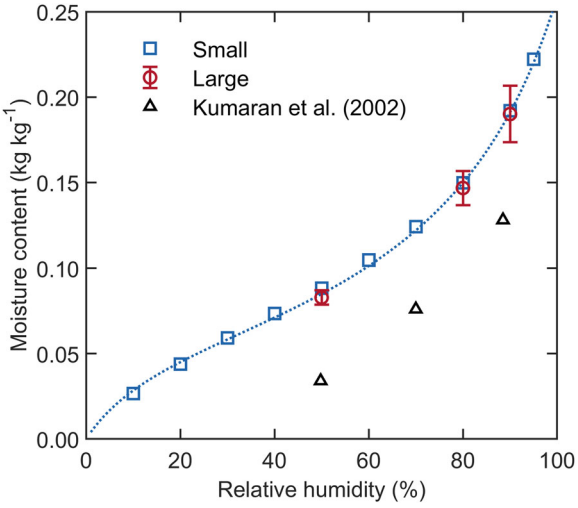

Fig. 8. Absorption equilibrium moisture content vs. relative humidity for small and large specimens of eastern white cedar in the hygroscopic range. Error bars represent standard deviation of six replicates of large specimens (omitted for small specimens and data of Kumaran et al. (2002) where standard deviations are smaller than the markers). Curve fit is based on combined data from this work.

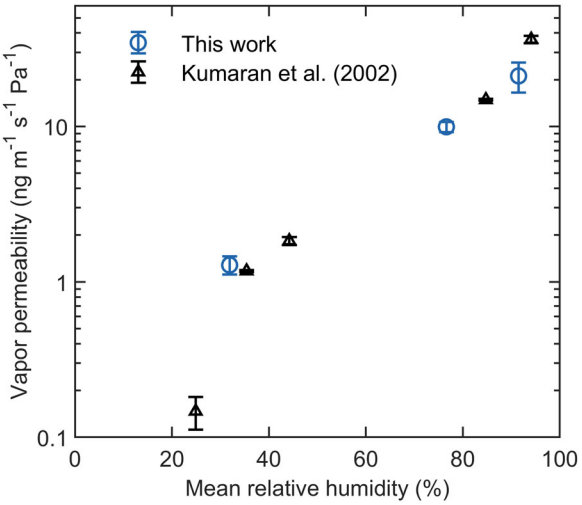

Fig. 9. Water vapor permeability of eastern white cedar vs. mean relative humidity. Error bars represent standard deviation of three replicates.

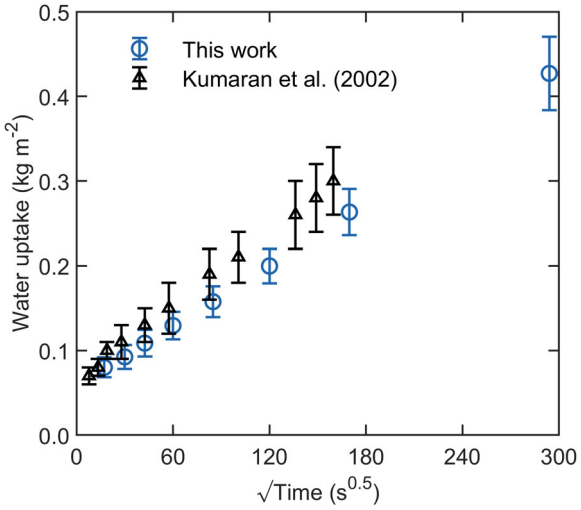

Fig. 10. Water uptake in eastern white cedar vs. square root of time. Error bars represent standard deviation of twelve replicates (this work) or four replicates (Kumaran et al. 2002).

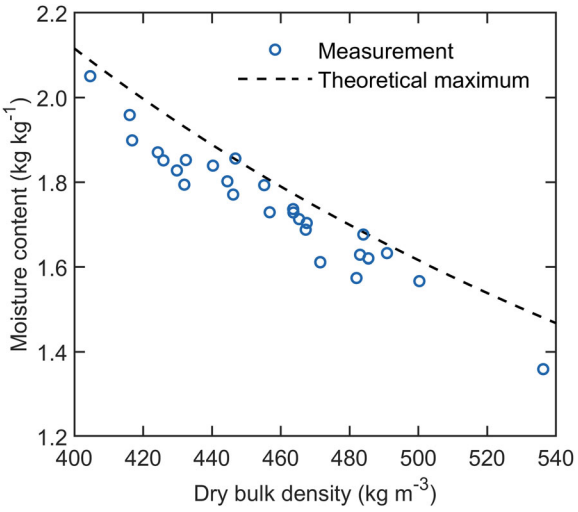

Fig. 11. Long duration free saturation vs. dry bulk density for southern yellow pine specimens. Theoretical maximum saturation is calculated from Equation (2).

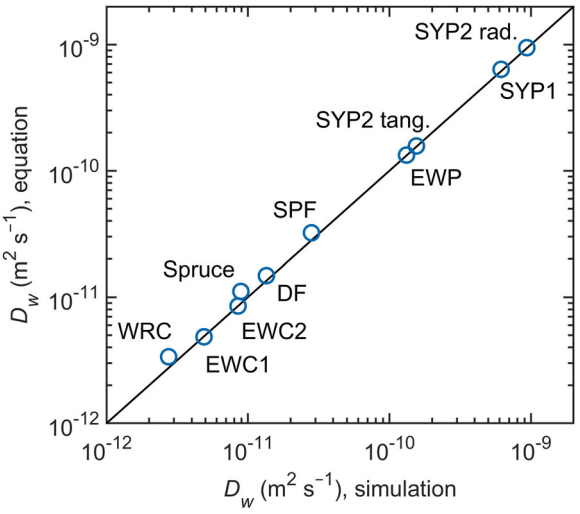

Fig. 12. Log-log plot of liquid diffusivity values for ten wood species calculated with Equation (14) vs. values calibrated by simulation. Solid line indicates $y = x$.

were still clearly absorbing water but at a miniscule rate after one year. Free saturation is thus not a practical method, except perhaps for very thin specimens that would reach saturation quickly. This is the case even for SYP, which is among the most water permeable wood species and is commonly used for pressure treatment with preservatives. Vacuum saturation for five days consistently gave lower moisture contents than long duration free saturation (not shown). These results, in conjunction with imaging studies of water absorption in softwoods (see Background/Capillary saturation), suggest that neither vacuum saturation nor free saturation provides relevant information about effective capillary saturation for the purpose of modeling water absorption in wood for building applications, where materials typically are exposed to intermittent wetting and drying rather than continuous wetting for long duration.

Model evaluation

The liquid diffusivity values calculated with Equation (14) are compared with the values calibrated by simulation in Figure 12. The ten data sets cover a range of North American softwood species spanning roughly three orders of magnitude in liquid diffusivity. Key properties of each wood species are summarized in Table 2, together with relative errors in liquid diffusivity. The optimized value of k in Equation (14) is 1.07 10^{-10} m^2 s^{-1}. The mean relative error is 8%, and six out of 10 species have $|e_j| < 4\%$. The species with the largest $|e_j|$ are spruce (25%) and western red cedar (23%), both of which have A values at the low end of the range and large contributions from vapor relative to liquid. At the opposite end of the range, EWP and the three sets of SYP have vapor contributions that are less than 5% of the respective liquid contributions; the mean relative error of this subgrouping (four out of 10 data sets) is 1.6%, indicating that the model performs well in the limit of vanishing vapor contribution. In other words, the model yields accurate results when the term containing its only empirical parameter becomes negligible.

The optimization in this study yields different values of liquid diffusivity than previous work (Glass, Boardman, and Daniels 2022), and mean relative error is reduced from 11% to 8% even though the current model has one less fitting parameter. The improved agreement between the model and calibrated simulations stems primarily from revising the moisture storage function based on literature data for absorption in the hygroscopic and over-hygroscopic range and setting the effective capillary saturation value to $0.9\rho_0$. The magnitude of the largest relative error is reduced from 63% (previously EWC) to 25% (Spruce). Eastern white cedar has thus changed from a potential outlier to one of the species with the lowest relative error. The model has a mean bias error of +7.8%; that is, Equation (14) overestimates D_w for most wood species relative to the calibrated simulations (Table 2).

The liquid diffusivity values found by calibrating the simulation to match the experimental water uptake are highly sensitive to the capillary saturation value. For example, reducing w_c for spruce by 10% from $0.9\rho_0$ (360 kg m^{-3}) to $0.8\rho_0$ (320 kg m^{-3}) increases the calibrated simulation D_w value by 23% from 8.91 10^{-12} m^2 s^{-1} to 1.10 10^{-11} m^2 s^{-1}. Given that the estimated value of $w_c = 0.9\rho_0$ is based on limited imaging data for Scots pine (see Background/Capillary saturation) and this property may vary depending on wood structure and chemistry, further research is recommended to identify capillary saturation values for absorption across the grain in a range of wood species with imaging techniques.

The impact of the improved liquid diffusivity model and updated material properties on simulated water uptake is shown in Figure 13 for two examples. In Figure 13a the measured data for spruce (Kumaran et al. 2002) over a duration of approximately 7.1 h is compared with the revised simulation using Equation (14) and the original simulation using the properties in the WUFI North America Database (IBP 2022), where liquid diffusivity is calculated using

Table 2. Liquid diffusivity and related properties of various wood species.

Wood species	ρ_0 (kg m^{-3})	A (g m^{-2} s$^{-0.5}$)	w_c (kg m^{-3})	μ_{90}	D_w (m^2 s^{-1}) simulation	D_w (m^2 s^{-1}) Equation (14)	e_i
EWC1	345	1.25	310	10.0	4.89 10^{-12}	4.85 10^{-12}	–0.8%
EWC2	360	1.45	324	10.0	8.51 10^{-12}	8.51 10^{-12}	0.0%
WRC	350	0.688	315	90.9	2.75 10^{-12}	3.37 10^{-12}	23%
EWP	460	4.98	414	20.4	1.32 10^{-10}	1.33 10^{-10}	0.6%
SYP1	500	11.7	450	12.3	6.15 10^{-10}	6.36 10^{-10}	3.4%
Spruce	400	1.87	360	7.1	8.91 10^{-12}	1.11 10^{-11}	25%
SYP2 rad.	445	12.7	400	7.5	9.35 10^{-10}	9.45 10^{-10}	1.0%
SYP2 tang.	445	5.26	400	14.0	1.55 10^{-10}	1.57 10^{-10}	1.2%
DF	477	2.08	429	14.0	1.35 10^{-11}	1.48 10^{-11}	10%
SPF	426	2.58	383	9.3	2.81 10^{-11}	3.22 10^{-11}	15%

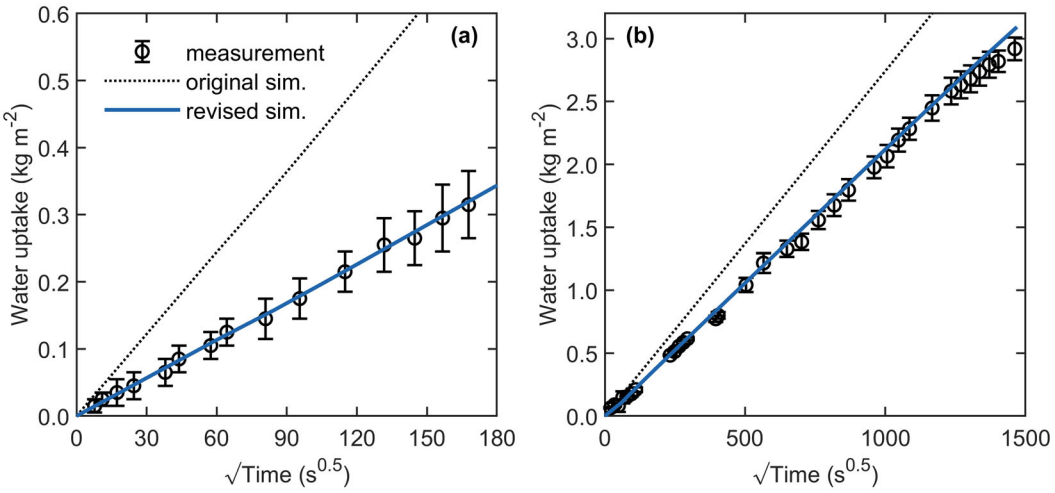

Fig. 13. Comparison of water absorption measurements and simulations: (a) data for spruce (Kumaran et al. 2002), original simulation using properties from the WUFI North America Database (IBP 2022), and revised simulation using properties from this work with liquid diffusivity from Equation (14); (b) data for Douglas-fir (Kordziel et al. 2020), original simulation using Equation (1), and revised simulation using Equation (14). Note the different horizontal and vertical axis scales.

Equation (1). In Figure 13b the simulations are compared with measurements for Douglas-fir (Kordziel et al. 2020), for which the duration was approximately 594 h (nearly 25 days). In this case the original simulation uses the liquid diffusivity approach of Equation (1) with the material properties reported by Kordziel et al. (2020), whereas the revised simulation uses Equation (14) with updated material properties. In both examples, the revised simulations compare favorably with measurements.

The engineering model for liquid diffusivity in wood presented in this article has several advantages: (a) it partitions liquid and vapor transport in a way that more closely aligns with the current understanding of wood–water interactions, thus avoiding double counting vapor diffusion and improving simulation accuracy; (b) it is practical and efficient to implement in hygrothermal models; (c) it is applicable to a broad range of North American softwoods; and (d) liquid diffusivity can be calculated directly from the water absorption coefficient, capillary saturation value, initial water content, and vapor diffusion resistance factor, so the method does not require moisture profile measurements or additional drying experiments. The model should be applicable to other softwood species that have water absorption coefficients and vapor diffusion resistance factors within the range of the species listed in Table 2.

The relative simplicity of the model, on the other hand, implies several limitations that need to be mentioned. The most reliable way of measuring capillary saturation is with advanced imaging methods such as NMR or neutron radiography, and data are scarce for water absorption in wood across the grain. Partial immersion tests are not practical for establishing capillary saturation in wood because water absorption is too slow. Vacuum saturation and free saturation give values that depend on the geometry of the specimen and the duration. Furthermore, laboratory vacuum conditions are not relevant for buildings in the real world, and free saturation values that take several months are not relevant for building materials exposed to intermittent precipitation. Given the scarcity of measured capillary saturation values, we relied on estimated values based on moisture profile data for Scots pine. In addition, the moisture storage function for most wood species at high RH did

not have enough data points to give the correct shape, so we inserted values based on reliable literature data. Our approach aimed to give a practical approximation rather than a detailed description of complexities such as non-linear water uptake vs. square root of time or the physical mechanism of water absorption at fine length and time scales.

We recommend further measurements of capillary saturation, equilibrium moisture content in the high RH range, moisture profiles during the water absorption process, and drying experiments to strengthen this simplified model. Although the scope of this study was restricted to modeling water absorption, we also recommend investigating whether the engineering model developed here could be extended to modeling liquid transport during drying and redistribution. Finally, given the appreciable inherent variation in properties within any wood species, sensitivity analysis is recommended to counter the risk of underpredicting water absorption in hygrothermal simulations.

Conclusions

This article presents an improved engineering model for liquid water absorption in softwoods across the grain. The approach directly addresses the partitioning between vapor and liquid transport in hygrothermal models. Prior approaches overpredict the rate of water absorption in wood because vapor diffusion is incorrectly assumed to be negligible during the water uptake measurement and is thus double counted in the simulation. Drawing on the current understanding of wood–water interactions, we argue that 99% RH is a reasonable threshold for capillary water transport and that an RH-dependent vapor diffusion resistance factor is a practical representation of combined diffusion of cell wall water and water vapor in the pore structure. Our approach for calculating liquid diffusivity builds on earlier approximations. For a given wood species, a single constant liquid diffusivity value is calculated based on the measured water absorption coefficient, estimated capillary saturation value, initial water content, and measured vapor diffusion resistance factor at 90% RH. The model uses one fitting parameter that is optimized across a range of North American softwood species from the literature using one-dimensional simulations. Liquid diffusivity values span roughly three orders of magnitude with a mean relative error of 8%. This practical approach improves simulation accuracy and primarily uses ordinary hygrothermal property measurements. Improvements over a previous version of the model stem from closer attention to the moisture storage function and capillary saturation value. Further work is recommended to test the approach with a broader set of experimental data including drying and redistribution, and to investigate capillary saturation and moisture storage at high RH levels for a broad range of wood species.

Nomenclature

A = water absorption coefficient (kg m^{-2} s$^{-0.5}$)
D = total water transport coefficient (m^2 s^{-1})
D_v = vapor transport coefficient (m^2 s^{-1})
D_w = liquid transport coefficient (m^2 s^{-1})
D_j^{eqn} = liquid transport coefficient for species j calculated with equation (m^2 s^{-1})
D_j^{cal} = liquid transport coefficient for species j calibrated by simulation (m^2 s^{-1})
e_j = relative error for species j (dimensionless)
$\bar{e}$ = mean relative error (dimensionless)
h = relative humidity (dimensionless)
k = empirical fitting parameter (m^2 s^{-1})
l = specimen thickness (m)
$\dot{m}$ = steady-state water vapor transmission rate (kg s^{-1})
p_v = water vapor pressure (Pa)
p_{vs} = saturation water vapor pressure (Pa)
S = surface area (m^2)
s_d = equivalent still air layer thickness for vapor diffusion resistance (m)
$U(t)$ = water uptake (kg m^{-2}) as a function of time
u = moisture content (kg kg^{-1})
u_{max} = maximum moisture content (kg kg^{-1})
w = water content (kg m^{-3})
$w(t)$ = average water content (kg m^{-3}) as a function of time
w_c = capillary saturation water content (kg m^{-3})
w_i = initial water content (kg m^{-3})
w_{max} = maximum water content (kg m^{-3})
x = distance (m)
δ_a = water vapor permeability of still air (kg m^{-1} s^{-1} Pa^{-1})
δ_p = water vapor permeability of material (kg m^{-1} s^{-1} Pa^{-1})
μ = water vapor diffusion resistance factor (dimensionless)
ρ_0 = dry bulk density (kg m^{-3})
φ = porosity (dimensionless)

Acknowledgements

The authors are grateful to Forest Products Laboratory colleagues Marshall Begel and Keith Bourne as well as anonymous reviewers for critical comments that improved the clarity of the article.

Disclosure statement

No potential conflict of interest was reported by the author(s).

Funding

This work was supported by the U.S. Department of Agriculture, Forest Service.

ORCID

Samuel V. Glass http://orcid.org/0000-0002-5451-1864
Charles R. Boardman http://orcid.org/0000-0002-9571-5601

Natalia Farkas http://orcid.org/0000-0002-7102-7345
Samuel L. Zelinka http://orcid.org/0000-0002-1348-7730

References

ASHRAE. 2019a. Building envelopes. In *ASHRAE handbook—HVAC applications, Ch. 45*. Atlanta: ASHRAE.

ASHRAE. 2019b. Moisture and mold. In *ASHRAE handbook—HVAC applications, Ch. 64*. Atlanta: ASHRAE.

ASHRAE. 2021a. *ANSI/ASHRAE Standard 160-2021, Criteria for moisture-control design analysis in buildings*. Atlanta: ASHRAE.

ASHRAE. 2021b. Heat, air, and moisture control in building assemblies—fundamentals. In *ASHRAE handbook—fundamentals, Ch. 25*. Atlanta: ASHRAE.

ASHRAE. 2021c. Moisture management in buildings. In *ASHRAE handbook—fundamentals, Ch. 37*. Atlanta: ASHRAE.

ASTM. 2016. *ASTM E3054/E3054M – 16, Standard guide for characterization and use of hygrothermal models for moisture control design in building envelopes*. West Conshohocken, PA: ASTM International.

ASTM. 2017. *ASTM D2395 – 17, standard test methods for density and specific gravity (relative density) of wood and wood-based materials*. West Conshohocken, PA: ASTM International.

ASTM. 2019. *ASTM C1794-19, standard test methods for determination of the water absorption coefficient by partial immersion*. West Conshohocken, PA: ASTM International.

Carmeliet, J., H. Janssen, and H. Derluyn. 2007. An improved moisture diffusivity model for porous building materials. In *Proceedings of 12th Symposium for Building Physics*; 2007 Mar 29–31. Dresden, Germany: Technical University of Dresden. p. 228–235.

Chen, M., B. Coasne, R. Guyer, D. Derome, and J. Carmeliet. 2018. Role of hydrogen bonding in hysteresis observed in sorption-induced swelling of soft nanoporous polymers. *Nature Communications* 9 (1):3507. doi:10.1038/s41467-018-05897-9.

Christensen, G. N., and K. E. Kelsey. 1959. The rate of sorption of water vapor by wood. *Holz Als Roh- Und Werkstoff* 17 (5):178–88. doi:10.1007/BF02608810.

Engelund, E. T., L. G. Thygesen, and P. Hoffmeyer. 2010. Water sorption in wood and modified wood at high values of relative humidity. Part 2: Appendix. Theoretical assessment of the amount of capillary water in wood microvoids. *Holzforschung* 64 (3):325–30. doi:10.1515/hf.2010.061.

Fortin, Y. 1979. Moisture content-matric potential relationship and water flow properties of wood at high moisture contents. PhD diss., Vancouver, Canada: University of British Columbia, Department of Forestry.

Fredriksson, M. 2019. On wood–water interactions in the over-hygroscopic moisture range—mechanisms, methods, and influence of wood modification. *Forests* 10 (9):779. doi:10.3390/f10090779.

Fredriksson, M., and P. Johansson. 2016. A method for determination of absorption isotherms at high relative humidity levels: Measurements on lime-silica brick and Norway spruce (*Picea abies* (L.) Karst.). *Drying Technology* 34 (1):132–41. doi:10.1080/07373937.2015.1041035.

Fredriksson, M., and E. E. Thybring. 2019. On sorption hysteresis in wood: Separating hysteresis in cell wall water and capillary water in the full moisture range. *PloS One* 14 (11):e0225111. doi:10.1371/journal.pone.0225111.

Gezici-Koç, Ö., S. J. F. Erich, H. P. Huinink, L. G. J. van der Ven, and O. C. G. Adan. 2017. Bound and free water distribution in wood during water uptake and drying as measured by 1D magnetic resonance imaging. *Cellulose* 24 (2):535–53. doi:10.1007/s10570-016-1173-x.

Glass, S. V., C. R. Boardman, E. E. Thybring, and S. L. Zelinka. 2018. Quantifying and reducing errors in equilibrium moisture content measurements with dynamic vapor sorption (DVS) experiments. *Wood Science and Technology* 52 (4):909–27. doi:10.1007/s00226-018-1007-0.

Glass, S. V., and S. L. Zelinka. 2021. Moisture relations and physical properties of wood. In *Wood handbook—wood as an engineering material (Chapter 4). General Technical Report FPL-GTR-282*. Madison, WI: U.S. Department of Agriculture, Forest Service, Forest Products Laboratory. https://www.fs.usda.gov/research/treesearch/62243.

Glass, S. V., S. L. Zelinka, and J. A. Johnson. 2014. *Investigation of historic equilibrium moisture content data from the forest products laboratory. General Technical Report FPL-GTR-229*. Madison, WI: US Department of Agriculture, Forest Service, Forest Products Laboratory. doi:10.2737/FPL-GTR-229.

Glass, S. V., C. R. Boardman, and E. Q. Daniels. 2022. Modeling water absorption in wood with an improved approximation method. In Proceedings, Thermal Performance of the Exterior Envelopes of Whole Buildings XV International Conference, Clearwater Beach, FL, Dec. 5–8, 2022, 347–356.

Greenspan, L. 1977. Humidity fixed points of binary saturated aqueous solutions. *Journal of Research of the National Bureau of Standards Section A: Physics and Chemistry* 81A (1):89–96. doi:10.6028/jres.081A.011.

Hedlin, C. P. 1967. Sorption isotherms of twelve woods at subfreezing temperatures. *Forest Products Journal* 17:43–8.

Hens, H. 1996. Final Report, Vol. 1, Task 1: Modelling. International Energy Agency Annex 24. –Heat, Air and Moisture Transfer through New and Retrofitted Insulated Envelope Parts (HAMTIE). Leuven, Belgium: Katholieke Universiteit Leuven.

IBP. 2022. *WUFI® Pro, version 6.6.0*. Holzkirchen, Germany: Fraunhofer Institute for Building Physics. https://wufi.de/en/

IOM. 2004. *Damp indoor spaces and health. U.S. Institute of Medicine*. Washington, DC: National Academies Press.

ISO. 2002. *ISO 15148:2002, Hygrothermal performance of building materials and products—determination of water absorption coefficient by partial immersion*. Geneva: International Organization for Standardization.

Jakes, J. E., C. G. Hunt, S. L. Zelinka, P. N. Ciesielski, and N. Z. Plaza. 2019. Effects of moisture on diffusion in unmodified wood cell walls: A phenomenological polymer science approach. *Forests* 10 (12):1084. doi:10.3390/f10121084.

Kordziel, S., S. V. Glass, C. R. Boardman, R. A. Munson, S. L. Zelinka, S. Pei, and P. C. Tabares-Velasco. 2020. Hygrothermal characterization and modeling of cross-laminated timber in the building envelope. *Building and Environment* 177:106866. doi:10.1016/j.buildenv.2020.106866.

Krus, M. 1996. *Moisture transport and storage coefficients of porous mineral building materials: Theoretical principles and new test methods*. Stuttgart: Fraunhofer IRB Verlag.

Krus, M., and T. A. Vik. 1999. Determination of hygric material properties and calculation of the moisture balance of wooden prisms. In 5th Symposium on Building Physics in the Nordic Countries, Gothenburg, Sweden, August 24–26, 1999.

Kulasinski, K., R. Guyer, D. Derome, and J. Carmeliet. 2015. Water diffusion in amorphous hydrophilic systems: A stop and go process. *Langmuir: The ACS Journal of Surfaces and Colloids* 31 (39):10843–9. doi:10.1021/acs.langmuir.5b03122.

Kumaran, M. K. 1999. Moisture diffusivity of building materials from water absorption measurements. *Journal of Thermal Envelope and Building Science* 22 (4):349–55. doi:10.1177/109719639902200409.

Kumaran, M. K., J. C. Lackey, N. Normandin, F. Tariku, and D. van Reenen. 2002. *A thermal and moisture transport property database for common building and insulating materials*. Final Report, ASHRAE Research Project 1018-RP. Atlanta: ASHRAE.

Künzel, H. M. 1995. *Simultaneous heat and moisture transport in building components: One- and two-dimensional calculation using simple parameters*. Stuttgart: Fraunhofer IRB Verlag.

Künzel, H. M., and K. Kiessl. 1997. Calculation of heat and moisture transfer in exposed building components. *International Journal of Heat and Mass Transfer* 40 (1):159–67. doi:10.1016/S0017-9310(96)00084-1.

Mendell, M. J., A. G. Mirer, K. Cheung, M. Tong, and J. Douwes. 2011. Respiratory and allergic health effects of dampness, mold, and dampness-related agents: A review of the epidemiologic evidence. *Environmental Health Perspectives* 119 (6):748–56. doi:10.1289/ehp.1002410.

Nopens, M., L. Wadsö, C. Ortmann, M. Fröba, and A. Krause. 2019. Measuring the heat of interaction between lignocellulosic materials and water. *Forests* 10(8): 674. doi:10.3390/f10080674

Plaza, N. Z. 2019. On the experimental assessment of the molecular-scale interactions between wood and water. *Forests* 10 (8):616. doi:10.3390/f10080616.

Sandberg, K., and J.-G. Salin. 2012. Liquid water absorption in dried Norway spruce timber measured with CT scanning and viewed as a percolation process. *Wood Science and Technology* 46 (1-3): 207–19. doi:10.1007/s00226-010-0371-1.

Scheffler, G., J. Grunewald, R. Plagge, P. Mukhopadhyaya, M. Kumaran, and S. W. Dean. 2007. Evaluation of functional approaches to describe the moisture diffusivity of building materials. *Journal of ASTM International* 4 (2):100498. doi:10.1520/JAI100498.

Sedighi-Gilani, M., M. Griffa, D. Mannes, E. Lehmann, J. Carmeliet, and D. Derome. 2012. Visualization and quantification of liquid water transport in softwood by means of neutron radiography. *International Journal of Heat and Mass Transfer* 55 (21-22): 6211–21. doi:10.1016/j.ijheatmasstransfer.2012.06.045.

Sedighi-Gilani, M., P. Vontobel, E. Lehmann, J. Carmeliet, and D. Derome. 2014. Liquid uptake in Scots pine sapwood and heartwood visualized and quantified by neutron radiography. *Materials and Structures* 47 (6):1083–96. doi:10.1617/s11527-013-0112-7.

Siau, J. F. 1984. *Transport processes in wood*. New York: Springer-Verlag.

Stamm, A. J. 1964. *Wood and cellulose science*. New York: The Ronald Press Company.

Straube, J. F., and E. F. P. Burnett. 2005. *Building science for building enclosures*. Westford, MA: Building Science Press.

Thybring, E. E., M. Fredriksson, S. L. Zelinka, and S. V. Glass. 2022. Water in wood: A review of current understanding and knowledge gaps. *Forests* 13 (12):2051. doi:10.3390/f13122051.

Thybring, E. E., S. V. Glass, and S. L. Zelinka. 2019. Kinetics of water vapor sorption in wood cell walls: State of the art and research needs. *Forests* 10 (8):704. doi:10.3390/f10080704.

Thygesen, L. G., E. T. Engelund, and P. Hoffmeyer. 2010. Water sorption in wood and modified wood at high values of relative humidity. Part I: Results for untreated, acetylated, and furfurylated Norway spruce. *Holzforschung* 64 (3):315–23. doi:10.1515/hf.2010.044.

Trechsel, H. R. ed. 2001. *Moisture analysis and condensation control in building envelopes, MNL 40*. West Conshohocken, PA: American Society for Testing and Materials.

Wadsö, L. 1994. Describing non-Fickian water-vapour sorption in wood. *Journal of Materials Science* 29 (9):2367–72. doi:10.1007/BF00363428.

WHO. 2009. *WHO guidelines for indoor air quality: Dampness and mould*. Copenhagen: World Health Organization.

Wiedenhoeft, A. C. 2021. Structure and function of wood. In: Wood handbook—wood as an engineering material (Chapter 3). In *General technical report FPL-GTR-282*. Madison, WI: U.S. Department of Agriculture, Forest Service, Forest Products Laboratory. https://www.fs.usda.gov/research/treesearch/62242.

Zelinka, S. L., K. J. Bourne, S. V. Glass, C. R. Boardman, L. Lorenz, and E. E. Thybring. 2018a. Apparatus for gravimetric measurement of moisture sorption isotherms for 1-100 g samples in parallel. *Wood and Fiber Science* 50 (3):244–53. doi:10.22382/wfs-2018-025

Zelinka, S. L., S. V. Glass, and C. R. Boardman. 2016a. Improvements to water vapor transmission and capillary absorption measurements in porous materials. *Journal of Testing and Evaluation* 44 (6):20150209. doi:10.1520/JTE20150209.

Zelinka, S. L., S. V. Glass, C. R. Boardman, and D. Derome. 2016b. Moisture storage and transport properties of preservative treated and untreated southern pine wood. *Wood Material Science & Engineering* 11 (4):228–38. doi:10.1080/17480272.2014.973443.

Zelinka, S. L., S. V. Glass, and E. E. Thybring. 2018b. Myth versus reality: Do parabolic sorption isotherm models reflect actual wood–water thermodynamics? *Wood Science and Technology* 52 (6):1701–6. doi:10.1007/s00226-018-1035-9.

Zelinka, S. L., M. J. Lambrecht, S. V. Glass, A. C. Wiedenhoeft, and D. J. Yelle. 2012. Examination of water phase transitions in Loblolly pine and cell wall components by differential scanning calorimetry. *Thermochimica Acta* 533:39–45. doi:10.1016/j.tca.2012.01.015.

Zillig, W. 2009. *Moisture transport in wood using a multiscale approach*. PhD diss., Leuven, Belgium: Katholieke Universiteit Leuven.

Supplementary Material

Journal: *Science and Technology for the Built Environment*

Improved engineering model for water absorption in softwoods

Samuel V. Glass*, Charles R. Boardman, Natalia Farkas, Eleanor Q.D. Lazarcik, and Samuel L. Zelinka

Building and Fire Sciences, USDA Forest Service, Forest Products Laboratory, Madison, Wisconsin, USA

*Corresponding author e-mail: samuel.v.glass@usda.gov

Contents

I. Water Uptake Simulations Using Original Properties

Water uptake in the five wood species from ASHRAE Research Project 1018 (Kumaran et al. 2002) was simulated using WUFI Pro software, version 6.6.0 (IBP 2022). Properties were directly assigned from the WUFI North America Database. These original properties are listed in Part III of the Supplementary Material.

The material thickness was 20 mm. The numerical parameters, initial conditions, and boundary conditions were the same as described in the *Water uptake simulations* section of *Materials and Methods* in the manuscript.

For the simulation with vapor diffusion excluded ("Liquid only" in Figure 2), the original material file was modified by setting the vapor diffusion resistance factor to a constant value of 100000.

For the simulation with liquid transport excluded ("Vapor only" in Figure 2), the original material file was used. In the "Hygrothermal Special Options" list under the "Numerics" menu, the box for "Excluding Capillary Conduction" was checked.

The simulated A-value for each wood species, based on the simulation with original properties, was identified as the slope of a linear regression of simulated total water content (kg m^{-2}) vs. square root of time ($s^{0.5}$) over the first eight hours, corresponding to the approximate duration of the measurements reported by Kumaran et al. (2002). Simulated and experimental A-values are compared in Table S1. The experimental A-value for each wood species in Table S1 was identified as the slope of a linear regression of water uptake vs. square root of time based on all data points from Kumaran et al. (2002).

Table S1. Experimental and simulated water absorption coefficients (original properties)

Wood species	A (kg m^{-2} $s^{-0.5}$)		Relative deviation
	Experimental[a]	Simulated	
Eastern White Cedar	0.00145	0.00351	142%
Eastern White Pine	0.00498	0.00716	44%
Southern Yellow Pine	0.0117	0.00237	–80%
Spruce	0.00187	0.00415	122%
Western Red Cedar	0.000688	0.00136	98%

[a] This analysis based on data from Kumaran et al. (2002)

Discrepancies were found between the experimental A-values calculated using the method described above ("this analysis") and those reported by Kumaran et al. (2002) based on the same measurements. The experimental A-values are compared in Table S2. The reason for the discrepancies is unclear; the analysis method used by Kumaran et al. (2002) is not documented. The values reported by Kumaran et al. (2002) are larger than those from this analysis except for Southern Yellow Pine, which appears to be a typographical error in the decimal place. The A-values reported by Kumaran et al. (2002) were directly used in the WUFI North America Database (IBP 2022) to generate the liquid transport coefficients for each wood species. The low A-value for Southern Yellow Pine explains why the original simulation underpredicts the measurements only in that case (indicated by a negative error in Table S1).

Table S2. Experimental water absorption coefficients reported by Kumaran et al. (2002) and from this analysis using the same data of Kumaran et al. (2002)

Wood species	A (kg m^{-2} s$^{-0.5}$)		Relative deviation
	Kumaran et al. (2002)	This analysis	
Eastern White Cedar	0.0016	0.00145	10%
Eastern White Pine	0.0066	0.00498	33%
Southern Yellow Pine	0.0014	0.0117	–88%
Spruce	0.0020	0.00187	7%
Western Red Cedar	0.0010	0.000688	45%

II. Maximum Water Saturation of Wood

Theoretical maximum water saturation u_{max} (kg kg^{-1}) can be calculated using the basic specific gravity G_b of wood:

$$u_{max} = \frac{1.54 - G_b}{1.54 G_b} \tag{S1}$$

where 1.54 is the approximate specific gravity of wood cell walls (Glass and Zelinka 2021). Basic specific gravity refers to mass in the ovendry state and volume in the saturated state. For hygrothermal simulations, the dry bulk density is typically used, and swelling and shrinking are neglected. Basic specific gravity relates to dry bulk density ρ_0 (kg m^{-3}) as follows (Glass and Zelinka 2021):

$$\rho_0 = \frac{1000 G_b}{1 - s_0} \tag{S2}$$

where s_0 is the total volumetric shrinkage from the saturated state to the ovendry state, expressed as a fraction of the volume in the saturated state. This quantity can be estimated from the basic specific gravity (Stamm 1964):

$$s_0 = 0.265 G_b \tag{S3}$$

Combining Eqs. (S1)–(S3) to eliminate G_b and s_0, theoretical maximum saturation is given by

$$u_{max} = \frac{1000}{\rho_0} - 0.3844 \tag{S4}$$

This can also be expressed as maximum water content w_{max} (kg m^{-3}):

$$w_{max} = 1000 - 0.3844 \rho_0 \tag{S5}$$

The porosity φ (= w_{max}/1000) can then be calculated as

$$\varphi = 1 - \frac{0.3844 \rho_0}{1000} \tag{S6}$$

III. Material Properties Used in Simulations

Material properties are listed below by wood species (see Table 1 of the manuscript for abbreviations) and include original properties from the WUFI North America Database (IBP 2022) as well as revised properties based on this work. The ABC isotherm equation for fitting sorption data can be found in Zelinka et al. (2018).

Eastern White Cedar

Table S3. General property data

Property	EWC1	EWC2, revised	EWC2, original [d]
Bulk density, dry (kg m^{-3})	345 [a]	360 [e]	360
Porosity (m^3 m^{-3})	0.8674 [b]	0.8616 [b]	0.82
Specific heat capacity, dry (J kg^{-1} K^{-1})	1237 [c]	1237 [c]	1880
Thermal conductivity, dry (W m^{-1} K^{-1})	0.0858 [c]	0.0885 [c]	0.091
Thermal conductivity temperature coefficient (W m^{-1} K^{-2})	0.0002 [d]	0.0002 [d]	0.0002
Thermal conductivity moisture coefficient (% $\%^{-1}$)	1.64 [c]	1.65 [c]	0

[a] This work; [b] Eq. (4); [c] Glass and Zelinka (2021); [d] WUFI North America Database (IBP 2022); [e] Kumaran et al. (2002)

Table S4. Moisture storage function

Relative humidity	Water content (kg m^{-3})		
	EWC1	EWC2, revised	EWC2, original [e]
0	0	0	0
0.1	9.2 [a]	9.6 [a]	
0.2	15.1 [a]	15.8 [a]	
0.3	20.4 [a]	21.3 [a]	
0.4	25.3 [a]	26.4 [a]	
0.499			9.36
0.5	29.2 [a]	30.5 [a]	
0.6	36.1 [a]	37.7 [a]	
0.7	42.8 [a]	44.7 [a]	
0.703			27
0.8	51 [a]	53.2 [a]	
0.886			44.64
0.9	65.8 [a]	68.7 [a]	
0.95	76.7 [a]	80 [a]	
0.99	86.3 [b]	90 [b]	
0.9992			633.6
0.99927	110.1 [c]	114.8 [c]	
0.99963	113.2 [c]	118.1 [c]	
0.99993	186.3 [c]	194.4 [c]	
1	310.5 [d]	324 [d]	750

[a] This work; [b] ABC isotherm fit to data from this work; [c] Fortin (1979); [d] Estimated as $0.9\rho_0$; [e] WUFI North America Database (IBP 2022)

Table S5. Liquid transport coefficient, suction

Water content (kg m^{-3})	DWS (m^2 s^{-1})		
	EWC1 [a]	EWC2, revised [a]	EWC2, original [b]
0	0	0	0
36.35			2.42×10^{-14}
86.3	4.89×10^{-12}		
90		8.51×10^{-12}	
310.5	4.89×10^{-12}		
324		8.51×10^{-12}	
750			2.73×10^{-11}

[a] Calibrated simulation; [b] WUFI North America Database (IBP 2022)

Table S6. Water vapor diffusion resistance factor

Relative humidity	μ-Value [a]		
	EWC1	EWC2, revised	EWC2, original
0	16515	16515	16515
0.1	16515	16515	16515
0.2	6648.2	6648.2	6648.2
0.3	2667.8	2667.8	2667.8
0.4	1072.6	1072.6	1072.6
0.5	429	429	429
0.6	172	172	172
0.7	68.2	68.2	68.2
0.8	26.6	26.6	26.6
0.9	10	10	10
1	10 [b]	10 [b]	3.3

[a] WUFI North America Database (IBP 2022) except as noted; [b] Constant above 90% RH

Western Red Cedar

Table S7. General property data

Property	WRC, revised	WRC, original [d]
Bulk density, dry (kg m^{-3})	350 [a]	350
Porosity (m^3 m^{-3})	0.8655 [b]	0.8
Specific heat capacity, dry (J kg^{-1} K^{-1})	1237 [c]	1880
Thermal conductivity, dry (W m^{-1} K^{-1})	0.0866 [c]	0.084
Thermal conductivity temperature coefficient (W m^{-1} K^{-2})	0.0002 [d]	0.0002
Thermal conductivity moisture coefficient (% $\%^{-1}$)	1.64 [c]	0

[a] Kumaran et al. (2002); [b] Eq. (4); [c] Glass and Zelinka (2021); [d] WUFI North America Database (IBP 2022)

Table S8. Moisture storage function

Relative humidity	Water content (kg m^{-3})	
	WRC, revised	WRC, original [d]
0	0	0
0.1	11.3 [a]	
0.2	16.8 [a]	
0.3	20.9 [a]	
0.4	24.8 [a]	
0.499		7.7
0.5	29 [a]	
0.6	33.9 [a]	
0.7	40 [a]	
0.703		26.25
0.8	48 [a]	
0.886		40.25
0.9	59.4 [a]	
0.95	67.2 [a]	
0.99	74.9 [a]	
0.9978		395.5
0.99927	111.7 [b]	
0.99963	114.8 [b]	
0.99993	189 [b]	
1	315 [c]	450

[a] ABC isotherm fit to data from Hedlin (1967); [b] Fortin (1979); [c] Estimated as $0.9\rho_0$; [d] WUFI North America Database (IBP 2022)

Table S9. Liquid transport coefficient, suction

Water content (kg m^{-3})	DWS (m^2 s^{-1})	
	WRC, revised [a]	WRC, original [b]
0	0	0
33.7		3.15×10^{-14}
74.9	2.75×10^{-12}	
315	2.75×10^{-12}	
450		1.88×10^{-11}

[a] Calibrated simulation; [b] WUFI North America Database (IBP 2022)

Table S10. Water vapor diffusion resistance factor

Relative humidity	μ-Value [a]	
	WRC, revised	WRC, original
0	1963	1963
0.1	1963	1963
0.2	1333.9	1333.9
0.3	912.7	912.7
0.4	621.2	621.2
0.5	423.8	423.8
0.6	288.6	288.6
0.7	196.3	196.3
0.8	133.4	133.4
0.9	90.9	90.9
1	90.9 [b]	61.4

[a] WUFI North America Database (IBP 2022) except as noted; [b] Constant above 90% RH

Eastern White Pine

Table S11. General property data

Property	EWP, revised	EWP, original [d]
Bulk density, dry (kg m^{-3})	460 [a]	460
Porosity (m^3 m^{-3})	0.8232 [b]	0.81
Specific heat capacity, dry (J kg^{-1} K^{-1})	1237 [c]	1880
Thermal conductivity, dry (W m^{-1} K^{-1})	0.1079 [c]	0.093
Thermal conductivity temperature coefficient (W m^{-1} K^{-2})	0.0002 [d]	0.0002
Thermal conductivity moisture coefficient (% $\%^{-1}$)	1.73 [c]	0

[a] Kumaran et al. (2002); [b] Eq. (4); [c] Glass and Zelinka (2021); [d] WUFI North America Database (IBP 2022)

Table S12. Moisture storage function

Relative humidity	Water content (kg m^{-3})	
	EWP, revised	EWP, original [d]
0	0	0
0.1	17.6 [a]	
0.2	23.7 [a]	
0.3	28.3 [a]	
0.4	33 [a]	
0.499		14.72
0.5	38.3 [a]	
0.6	44.8 [a]	
0.7	53.5 [a]	
0.703		38.18
0.8	65.7 [a]	
0.886		56.12
0.9	84.6 [a]	
0.95	98.5 [a]	
0.99	113.3 [a]	
0.9978		386.4
0.99927	146.7 [b]	
0.99963	150.9 [b]	
0.99993	248.4 [b]	
1	414 [c]	450

[a] ABC isotherm fit from Glass et al. (2014); [b] Fortin (1979); [c] Estimated as $0.9\rho_0$; [d] WUFI North America Database (IBP 2022)

Table S13. Liquid transport coefficient, suction

Water content (kg m^{-3})	DWS (m^2 s^{-1})	
	EWP, revised [a]	EWP, original [b]
0	0	0
47.7		1.7×10^{-12}
113.3	1.32×10^{-10}	
414	1.32×10^{-10}	
450		8.17×10^{-10}

[a] Calibrated simulation; [b] WUFI North America Database (IBP 2022)

Table S14. Water vapor diffusion resistance factor

Relative humidity	μ-Value [a]	
	EWP, revised	EWP, original
0	4427.4	4427.4
0.1	4427	4427
0.2	2276.7	2276.7
0.3	1169	1169
0.4	601.4	601.4
0.5	308.7	308.7
0.6	158.8	158.8
0.7	80.7	80.7
0.8	41	41
0.9	20.4	20.4
1	20.4 [b]	9.9

[a] WUFI North America Database (IBP 2022) except as noted; [b] Constant above 90% RH

Southern Yellow Pine

Table S15. General property data

Property	SYP1, revised	SYP1, original [d]	SYP2 rad./tang.
Bulk density, dry (kg m^{-3})	500 [a]	500	445 [e]
Porosity (m^3 m^{-3})	0.8078 [b]	0.858	0.8289 [b]
Specific heat capacity, dry (J kg^{-1} K^{-1})	1237 [c]	1880	1237 [c]
Thermal conductivity, dry (W m^{-1} K^{-1})	0.1157 [c]	0.119	0.105 [c]
Thermal conductivity temperature coefficient (W m^{-1} K^{-2})	0.0002 [d]	0.0002	0.0002 [d]
Thermal conductivity moisture coefficient (% $\%^{-1}$)	1.76 [c]	0	1.72 [c]

[a] Kumaran et al. (2002); [b] Eq. (4); [c] Glass and Zelinka (2021); [d] WUFI North America Database (IBP 2022); [e] Zelinka et al. (2016)

Table S16. Moisture storage function

Relative humidity	Water content (kg m^{-3})		
	SYP1, revised	SYP1, original [d]	SYP2 rad./tang.
0	0	0	0
0.1	19.2 [a]		17.1 [a]
0.2	25.8 [a]		22.9 [a]
0.3	30.8 [a]		27.4 [a]
0.4	35.8 [a]		31.9 [a]
0.499		20	
0.5	41.6 [a]		37 [a]
0.6	48.7 [a]		43.4 [a]
0.7	58.2 [a]		51.8 [a]
0.703		45.5	
0.8	71.5 [a]		63.6 [a]
0.886		77	
0.9	92 [a]		81.8 [a]
0.95	107.1 [a]		95.3 [a]
0.99	123.2 [a]		109.6 [a]
0.9978		285	
0.99927	159.5 [b]		142 [b]
0.99963	164 [b]		146 [b]
0.99993	270 [b]		240.3 [b]
1	450 [c]	300	400.5 [c]

[a] ABC isotherm fit from Glass et al. (2014); [b] Fortin (1979); [c] Estimated as $0.9\rho_0$; [d] WUFI North America Database (IBP 2022)

Table S17. Liquid transport coefficient, suction

Water content (kg m^{-3})	DWS (m^2 s^{-1})			
	SYP1, revised [a]	SYP1, original [b]	SYP2 rad. [a]	SYP2 tang. [a]
0	0	0	0	0
62.2		3.47×10^{-13}		
109.6			9.35×10^{-10}	1.55×10^{-10}
123.2	6.15×10^{-10}			
300		8.28×10^{-11}		
400.5			9.35×10^{-10}	1.55×10^{-10}
450	6.15×10^{-10}			

[a] Calibrated simulation; [b] WUFI North America Database (IBP 2022)

Table S18. Water vapor diffusion resistance factor

Relative humidity	μ-Value			
	SYP1, revised [a]	SYP1, original [a]	SYP2 rad. [c]	SYP2 tang. [c]
0	1734.1	1734.1	56	166
0.1	1734	1734		
0.2	945.9	945.9		
0.3	515.1	515.1		
0.31			56	166
0.4	280	280		
0.5	151.9	151.9		
0.6	82.2	82.2		
0.7	44.3	44.3		
0.725			16	32
0.8	23.6	23.6		
0.89			8	15
0.9	12.3	12.3	7.5	14
1	12.3 [b]	6.1	7.5 [b]	14 [b]

[a] WUFI North America Database (IBP 2022) except as noted; [b] Constant above 90% RH; [c] Zelinka et al. (2016) except as noted

Spruce

Table S19. General property data

Property	Spruce, revised	Spruce, original [d]
Bulk density, dry (kg m^{-3})	400 [a]	400
Porosity (m^3 m^{-3})	0.8462 [b]	0.9
Specific heat capacity, dry (J kg^{-1} K^{-1})	1237 [c]	1880
Thermal conductivity, dry (W m^{-1} K^{-1})	0.0963 [c]	0.086
Thermal conductivity temperature coefficient (W m^{-1} K^{-2})	0.0002 [d]	0.0002
Thermal conductivity moisture coefficient (% $\%^{-1}$)	1.69 [c]	0

[a] Kumaran et al. (2002); [b] Eq. (4); [c] Glass and Zelinka (2021); [d] WUFI North America Database (IBP 2022)

Table S20. Moisture storage function

Relative humidity	Water content (kg m^{-3})	
	Spruce, revised	Spruce, original [d]
0	0	0
0.1	14.4 [a]	
0.2	20.7 [a]	
0.3	25.6 [a]	
0.4	30.4 [a]	
0.499		18
0.5	35.9 [a]	
0.6	42.6 [a]	
0.7	51.7 [a]	
0.703		41.2
0.8	64.6 [a]	
0.886		68.8
0.9	85.1 [a]	
0.95	100.7 [a]	
0.99	117.9 [a]	
0.9978		748
0.99927	127.6 [b]	
0.99963	131.2 [b]	
0.99993	216 [b]	
1	360 [c]	845

[a] ABC isotherm fit to data from Hedlin (1967); [b] Fortin (1979); [c] Estimated as $0.9\rho_0$; [d] WUFI North America Database (IBP 2022)

Table S21. Liquid transport coefficient, suction

Water content (kg m^{-3})	DWS (m^2 s^{-1})	
	Spruce, revised [a]	Spruce, original [b]
0	0	0
55.8		3.35×10^{-14}
117.9	8.91×10^{-12}	
360	8.91×10^{-12}	
845		2.13×10^{-11}

[a] Calibrated simulation; [b] WUFI North America Database (IBP 2022)

Table S22. Water vapor diffusion resistance factor

Relative humidity	μ-Value [a]	
	Spruce, revised	Spruce, original
0	552	552
0.1	552	552
0.2	326.2	326.2
0.3	192.7	192.7
0.4	113.1	113.1
0.5	66.5	66.5
0.6	38.8 [b]	28.8
0.7	22.4	22.4
0.8	12.8	12.8
0.9	7.1	7.1
1	7.1 [c]	3.7

[a] WUFI North America Database (IBP 2022) except as noted; [b] Correction of apparent typographical error; [c] Constant above 90% RH

Douglas-Fir and Western Spruce-Pine-Fir Group

Table S23. General property data

Property	DF	SPF
Bulk density, dry (kg m^{-3})	477 [a]	426 [a]
Porosity (m^3 m^{-3})	0.8166 [b]	0.8362 [b]
Specific heat capacity, dry (J kg^{-1} K^{-1})	1237 [c]	1237 [c]
Thermal conductivity, dry (W m^{-1} K^{-1})	0.1112 [c]	0.1013 [c]
Thermal conductivity temperature coefficient (W m^{-1} K^{-2})	0.0002 [d]	0.0002 [d]
Thermal conductivity moisture coefficient (% $\%^{-1}$)	1.74 [c]	1.71 [c]

[a] Kordziel et al. (2020); [b] Eq. (4); [c] Glass and Zelinka (2021); [d] WUFI North America Database (IBP 2022)

Table S24. Moisture storage function

Relative humidity	Water content (kg m^{-3})	
	DF	SPF
0	0	0
0.1	15.4 [a]	15.5 [a]
0.2	22.8 [a]	22 [a]
0.3	28.6 [a]	27 [a]
0.4	34.2 [a]	32 [a]
0.5	40.4 [a]	37.7 [a]
0.6	48 [a]	44.8 [a]
0.7	57.9 [a]	54.2 [a]
0.8	71.8 [a]	67.9 [a]
0.9	93.2 [a]	89.8 [a]
0.95	109.1 [a]	106.7 [a]
0.99	126 [a]	125.3 [a]
0.99927	152.2 [b]	135.9 [b]
0.99963	156.5 [b]	139.7 [b]
0.99993	257.6 [b]	230 [b]
1	429.3 [c]	383.4 [c]

[a] ABC isotherm fit to combined data from Hedlin (1967) and Kordziel et al. (2020); [b] Fortin (1979); [c] Estimated as $0.9\rho_0$

Table S25. Liquid transport coefficient, suction

Water content (kg m^{-3})	DWS (m^2 s^{-1}) [a]	
	DF	SPF
0	0	0
125.3		2.81×10^{-11}
126	1.35×10^{-11}	
383.4		2.81×10^{-11}
429.3	1.35×10^{-11}	

[a] Calibrated simulation

Table S26. Water vapor diffusion resistance factor

Relative humidity	μ-Value [a]	
	DF	SPF
0	171.33	145.53
0.25	171.33	145.53
0.5	64.84	50.58
0.75	24.86	17.52
0.9	13.99	9.27
1	13.99 [b]	9.27 [b]

[a] Kordziel et al. (2020) except as noted; [b] Constant above 90% RH

References

Fortin, Y. 1979. *Moisture content-matric potential relationship and water flow properties of wood at high moisture contents*. Ph.D. dissertation. Vancouver, Canada: University of British Columbia, Department of Forestry.

Glass, S.V., and S.L. Zelinka. 2021. Moisture relations and physical properties of wood. In: Wood handbook—wood as an engineering material (Chapter 4). General Technical Report FPL-GTR-282. Madison, WI: U.S. Department of Agriculture, Forest Service, Forest Products Laboratory. https://www.fs.usda.gov/research/treesearch/62243

Glass, S.V.; Zelinka, S.L.; Johnson, J.A. 2014. Investigation of historic equilibrium moisture content data from the Forest Products Laboratory. General Technical Report FPL-GTR-229. Madison, WI: US Department of Agriculture, Forest Service, Forest Products Laboratory. https://doi.org/10.2737/FPL-GTR-229

Hedlin, C.P. 1967. Sorption isotherms of twelve woods at subfreezing temperatures. *Forest Products Journal* 17: 43–48.

IBP. 2022. WUFI® Pro, version 6.6.0. Holzkirchen, Germany: Fraunhofer Institute for Building Physics. https://wufi.de/en/

Kordziel, S., Glass, S.V., Boardman, C.R., Munson, R.A., Zelinka, S.L., Pei, S., and P.C. Tabares-Velasco. 2020. Hygrothermal characterization and modeling of cross-laminated timber in the building envelope. *Building and Environment* 177: 106866. https://doi.org/10.1016/j.buildenv.2020.106866

Kumaran, M.K., Lackey, J.C., Normandin, N., Tariku, F., and D. van Reenen. 2002. *A thermal and moisture transport property database for common building and insulating materials*. Final Report, ASHRAE Research Project 1018-RP. Atlanta: ASHRAE.

Stamm, A.J. 1964. *Wood and cellulose science*. New York: The Ronald Press Company.

Zelinka, S.L., Glass, S.V., Boardman, C.R., and D. Derome. 2016. Moisture storage and transport properties of preservative treated and untreated southern pine wood. *Wood Material Science and Engineering* 11(4): 228–238. https://doi.org/10.1080/17480272.2014.973443

Zelinka, S.L., Glass, S.V., and E.E. Thybring. 2018. Myth versus reality: Do parabolic sorption isotherm models reflect actual wood–water thermodynamics? *Wood Science and Technology* 52(6): 1701–1706. https://doi.org/10.1007/s00226-018-1035-9